(2)

REPORT RE-804

AN INVESTIGATION OF THE FUNDAMENTAL CAUSE OF ASYMMETRIC SEPARATED FLOW

NOVEMBER 1992

prepared by

F. Marconi
Grumman Aerospace Corporation
Bethpage, New York 11714

Final Report on Contract DAAL03-91-C-0013
for Period 1 April 1991 - 30 June 1992

prepared for

ARMY RESEARCH OFFICE
P. O. BOX 12211
Research Triangle Park, NC 27709-2211

Approved by: _____
Richard De Iasi, Director
Corporate Research Center

REPORT DOCUMENTATION PAGE

Form Approved
OMB No. 0704-0188

1. AGENCY USE ONLY (Leave blank)	2. REPORT DATE	3. REPORT TYPE AND DATES COVERED
	October 1992	

4. TITLE AND SUBTITLE
An Investigation of the Fundamental Cause of Asymmetric Separated Flow

5. FUNDING NUMBERS
DAAL03-91-C-0013

6. AUTHOR(S)
F. Marconi

7. PERFORMING ORGANIZATION NAME(S) AND ADDRESS(ES)
Grumman Aerospace Corporation
Bethpage, NY 11714

8. PERFORMING ORGANIZATION REPORT NUMBER

9. SPONSORING/MONITORING AGENCY NAME(S) AND ADDRESS(ES)
U. S. Army Research Office
P. O. Box 12211
Research Triangle Park, NC 27709-2211

10. SPONSORING/MONITORING AGENCY REPORT NUMBER
ARO 28252.1-EG

11. SUPPLEMENTARY NOTES
The view, opinions and/or findings contained in this report are those of the author(s) and should not be conatrued as an official Department of the Army position, policy, or decision, unless so designated by other documentation.

12a. DISTRIBUTION/AVAILABILITY STATEMENT
Approved for public release; distribution unlimited.

12b. DISTRIBUTION CODE

13. ABSTRACT *(Maximum 200 words)*

The cause of the phenomenon of steady asymmetric flow on cones at moderately high angles of attack is the subject of this investigation. At very higher angles of attack, the flow will become unsteady with a Karman vortex street being shed downstream. This second phenomenon was not considered in the current research project. The investigation used computational fluid dynamics as a tool to uncover the fundamental cause of asymmetric separated flows. The appearance of new flow features as the critical angle of attack was approached was studied in detail. Isolating asymmetric disturbances to specific portions of the flow was also attempted. The stability of the symmetric flow above the critical angle of attack was investigated analytically. The transition of the flow from symmetric to asymmetric as the computation was continued was studied in detail. All of these studies indicated that the interaction of the vortices in the cross flow plane results in an instability in the symmetric flow. In addition, the interaction between the vortices seems to be somewhat global in nature.

14. SUBJECT TERMS	15. NUMBER OF PAGES
Vortex Flows, Asymmetric Flows, High Angle of Attack Flows	47
	16. PRICE CODE

17. SECURITY CLASSIFICATION OF REPORT	18. SECURITY CLASSIFICATION OF THIS PAGE	19. SECURITY CLASSIFICATION OF ABSTRACT	20. LIMITATION OF ABSTRACT
UNCLASSIFIED	UNCLASSIFIED	UNCLASSIFIED	UL

NSN 7540-01-280-5500

Standard Form 298 (Rev 2-89)
Prescribed by ANSI Std Z39-18
298-102

DISCLAIMER NOTICE

THIS DOCUMENT IS BEST QUALITY AVAILABLE. THE COPY FURNISHED TO DTIC CONTAINED A SIGNIFICANT NUMBER OF COLOR PAGES WHICH DO NOT REPRODUCE LEGIBLY ON BLACK AND WHITE MICROFICHE.

FOREWORD

As a slender-nosed vehicle (aircraft or missile) flies at higher angles of incidence, the lee flow which is attached at low angle of attack becomes separated and two counter-rotating vortices are formed. If the angle of incidence of the vehicle is below the slender-nose included angle, these vortices will be symmetric with respect to the geometric symmetry plane as long as the free-stream velocity vector remains in this plane. At angles of attack higher than a critical value (approximately the nose included angle), the separation vortices can become asymmetric even though the free-stream velocity is in the geometric symmetry plane. The cause of this phenomenon is the subject of this investigation. At even higher angles of attack, the flow will become unsteady with a Karman vortex street being shed downstream. This second phenomenon was not considered in the current research project. The investigation used computational fluid dynamics as a tool to uncover the fundamental cause of asymmetric separated flows. The appearance of new flow features as the critical angle of attack was approached was studied in detail. Isolating asymmetric disturbances to specific portions of the flow was also attempted. The stability of the symmetric flow above the critical angle of attack was investigated analytically. Finally, the transition of the flow from symmetric to asymmetric as the computation was continued was studied in detail. All of these studies indicated that the interaction of the vortices in the cross flow plane results in an instability in the symmetric flow, and only an asymmetry can stabilize the flow. The findings of this research have localized the instability to the lee plane region of the flow but it can not be isolated to any particular singular point. The interaction between the vortices seems to be the cause of the instability, and this interaction is somewhat global in nature.

TABLE OF CONTENTS

LIST OF ILLUSTRATIONS

1. BACKGROUND

High angle-of-attack maneuvering demands on both aircraft and missiles make the phenomenon of asymmetric separated flows of primary concern. Since the late 1940s, it has been known that the sudden onset of asymmetric vortex flow is the cause of an unexpected and significant yawing force experienced by slender-nosed aircraft. As a slender-nosed missile or aircraft is pitched through increasing angles of attack, the flow that had been symmetric about the plane containing the free-stream velocity vector can suddenly become asymmetric. It has been found experimentally that this is related to the vortices that spring from the separation points and sit above the nose near the lee plane of "symmetry." Below a critical angle of attack, the lee plane is indeed a plane about which the flow is symmetric. Once beyond the critical angle of attack, these separation vortices suddenly become asymmetrically disposed. At even higher angles of attack, the flow will become unsteady, and the vortices will be shed and carried downstream periodically as in a Karman vortex street. In this research, only steady asymmetric flows were studied, and angles of attack much greater than the critical value were not considered.

The surface pressure distribution is related very closely to vortex strength and location near the lee plane, so that once the vortices become asymmetric, so does the surface pressure. This asymmetric surface pressure results in a side force which, because of its sudden onset, can create control problems for a vehicle. Currently, there are a number of studies in this country directed toward harnessing this side force for lateral control augmentation. At angles of attack near 40 deg, the vertical tail of an aircraft is in the separation zone of the wings so that the rudder is somewhat ineffective as a lateral control device. If the aircraft is to maneuver at these angles of attack, another source of side force must be found. If the onset, directionality, and degree of asymmetric vortex flow can be controlled, the resulting side force can be used to supplement rudder control at high angle of attack.

Ever since asymmetric separation was first discovered, its fundamental cause has been debated. Experimentalists have, over the years, been able to affect and control the phenomenon to some extent (Ref 1). They have found that blunting the nose of slender vehicles delays, in terms of angle of attack, the onset of side force (Ref 2). Strakes have been used quite effectively in almost eliminating this

phenomenon (Ref 3). Tangential blowing has also been used to control the asymmetry (Ref 4). It has been found that Reynolds number effects are limited to the turbulent state of the flow. These effects are significant but are confined to the separation pattern of the cross-flow (Ref 5). Increasing Mach number reduces the side force significantly, all other parameters being fixed (Ref 6). None of these experimental studies have addressed the fundamental cause of the anomaly. Over the past ten years, a number of computational/analytical studies have been presented. The work at the RAE (Ref 7) with a simple vortex line model was a breakthrough in understanding this phenomenon. Dyer, Fiddes, and Smith (Ref 7) found a bifurcation in the solution to the small disturbance equations combined with Bryson's (Ref 8) simple vortex line model. This model is irrotational everywhere except at an infinitesimal feeding vortex sheet that springs from specified separation point locations. Below a critical angle of attack there is only one solution, its vortices symmetrically located about the lee plane as long as the separation points are symmetric. Above the critical angle of attack there are three solutions: the symmetric (as long as the specified separation points are symmetric) and two mirror image asymmetric solutions. This analytical/computational result indicates that the phenomenon is natural, i. e., not due to any experimental inaccuracies and, in fact, is controlled by a purely inviscid mechanism. Fiddes extended this work by replacing the line vortices by vortex sheets (Ref 9). He found the same bifurcation at a critical angle of attack.

Using the Kutta condition development at RAE (Ref 10) the present author was able to predict separated flows with an Euler model. The condition was modified and applied successfully to primary and secondary separation, on cones (Ref 11) delta wings (Ref 12), and cone cylinders (Ref 13) at high angle of attack and supersonic speeds. More importantly, it was found that if the symmetry condition was relaxed, the supersonic flow over a cone with separation modeled via a Kutta condition could become asymmetric. As a matter of fact, unlike the small disturbance results of Fiddes, the Euler equations predicted that the symmetric solution was impossible to compute to convergence, and only the two mirror image asymmetric results were obtained. These findings were published in the 10th International Conference on Numerical Methods in Fluid Dynamics (Ref 14).

Both the small disturbances and Euler models require the locations of separation to be specified. The locations are dependent upon the detail of the

viscid/inviscid interaction. The interaction and the resulting separation location can be determined by solving the Navier-Stokes equation. Siclari and Marconi (Ref 15) were able to obtain "locally conical" steady laminar Navier-Stokes full-plane solutions for a 5-deg cone at a supersonic Mach number of 1.8 that exhibited a continuous range of naturally occurring bifurcated solutions without the imposition of a viscous separation model, geometric perturbation, or asymmetric boundary condition. Unlike other studies (Ref 16), it was found in Ref 15 that the asymmetric conical viscous solutions could be achieved naturally without any geometric irregularities or other perturbations to maintain them. These naturally occurring "locally conical" asymmetric solutions were verified by other investigations such as Kandil, Wong, and Liu (Ref 17) and Rosen and Davis (Ref 18) using other viscous codes. Thomas (Ref 18) performed a detailed study of the effect of local Reynolds number on the computation of these conical flows. It was found that the asymmetry is reduced as the Reynolds number is decreased, to the point where the side force which was comparable to the normal force at $Re_L=10^6$ is insignificant at $Re_L=3x10^4$.

This naturally occurring phenomenon may be distinct from another phenomenon noted by Degani and Schiff (Ref 18) where small geometric or other flow perturbations at the apex may trigger or be amplified into a more global asymmetric flow behavior. Hartwich et al. (Ref 18) recently found both phenomena. First, Navier-Stokes solutions were obtained that exhibited asymmetries with no asymmetric perturbation maintained. Then Hartwich showed how small geometric perturbations at the nose of a cone/cylinder can be amplified. These phenomena have been noted experimentally for a number of years. Recent experimental studies have indicated two angle-of-attack regimes where steady asymmetric flow exists. In the lower regime, the asymmetric flow is amplifying small geometric asymmetries at the vehicle nose. At the higher angles of attack, the nose asymmetries do not control the flow asymmetry. It is this higher angle-of-attack regime where the naturally occurring asymmetric flow exists. Samples of such experiments can be found in Ref 18 and 22. In Ref 21, a cone cylinder is rolled about its axis at a constant high angle of attack. A continuous variation in side force was measured, indicating that the asymmetries are being controlled by a slight geometric asymmetry at the nose. When the angle of attack was increased further, the flow remained steady and an unstable situation was encountered. The side force exhibited only two values (one the negative of the other) as the model was rolled. This indicates that while small geometric irregularities may be triggering the asymmetry, there is a basic instability in the flow field.

Computationally, this would manifest itself by an instability in the symmetric solution. Above a critical angle of attack, the only way to maintain a symmetric solution is to impose symmetry. Arbitrarily small perturbations, either truncation or even machine round-off error, will push the symmetric solution to one of the stable mirror image asymmetric flows. Both the Euler and Navier-Stokes conical flow solutions have exhibited this phenomenon (see Ref 14 and 15, for example).

When started from symmetric initial conditions, the conical solutions presented in Ref 15 would be driven to the symmetric solution until the residuals approached the truncation error of the machine. At this point, the residual would rise almost to its original level and then diminish again and finally converge to machine zero. The solution would then converge to one of the two mirror image asymmetric solutions. It was also discovered that the solution could be driven directly to the asymmetric solution by specifying asymmetric initial conditions. In the first case, truncation error was the asymmetric trigger, while in the second, it was the asymmetric initial conditions. The solutions presented in Ref 15 indicated the sudden onset of bifurcated, asymmetric, solutions at a critical ratio of incidence to cone half angle of somewhat greater than two. It was also discovered that with increasing incidence the side force peaked, and then the bifurcated asymmetric solutions rapidly returned to a single symmetric one with further increase in incidence.

It was the intent of the current research project to uncover the root cause of asymmetric separated conical flow. The possibility that a flow singularity was related to the first occurrence of the phenomenon was investigated. There was some evidence that the first appearance of a saddle/node combination signaled the instability in the symmetric flow. In particular, this seems to be the case for circular cones. The study, the details of which are presented in Section 2.1, indicates that the occurrence of the node/saddle and the instability become significantly different for cross sections other than circular. An analysis of different regions of the flow field presented in Section 2.2 indicated that while only the region near the lee plane was unstable, above the critical angle of attack the instability couldn't be isolated any farther than a region containing the two vortex cores. An Orr-Sommerfeld local stability analysis (see Section 2.3) failed, indicating again that the instability was cause by a somewhat global phenomenon. This was substantiated by a detailed study in the flow as it transitioned from symmetric to asymmetric. This is discussed in Section 2.4. The findings of this research are summarized in Section 3. Appendix A

presents results not directly related to the cause of asymmetric separation but to the effect of nose tip spinning on this phenomenon.

2. RESULTS OF THE INVESTIGATIONS

The work horse of this investigation was a conical Navier-Stokes solver. The flow considered here is supersonic, so that if the geometry is self similar with respect to its axis and the flow is assumed inviscid, all variables would be independent of the spherical coordinate (R, Fig. 1). This results in a conical computation, i. e., two-dimensional in the cross-flow plane (R = constant). The first computational results demonstrating asymmetric separation -- the small disturbance calculation [7] and the Euler results [14] -- were both two-dimensional in the cross-flow plane. The small disturbance assumption neglects derivatives in the axial (z, Fig. 1) direction resulting in the two-dimensional Laplace's equation in the cross-flow plane whether the free steam is supersonic or subsonic. In the case of the fully nonlinear Euler model, as long as there is no upstream influence (i. e., the flow remains supersonic) and the separation lines are straight, the flow is absolutely conical. Both the models are inviscid, requiring the specification of the separation line location. In some sense it was this restriction on the models which shed light on the phenomenon of asymmetric separation because the anomaly first appeared with symmetrically specified separation points. This indicates that the instability in the symmetric flow above the critical angle of attack in inherently inviscid. These two computational models demonstrated clearly that the phenomenon under consideration here is both inviscid and conical. The viscous terms are added in the calculation used here in order to avoid the requirement of specifying separation line location while the conical assumption is retained to keep the computation two dimensional. Keeping the computation two dimensional enabled the investigation to be carried out with a minimum of concern for numerical inaccuracy. Very fine grids (58 points in the r direction and 96 in the θ direction, Fig. 1) were used throughout this study and all calculations were continued until the residual in the iteration scheme reached machine zero. It has been demonstrated (Ref 15) that both these issues are very important in the flows considered here. On today's supercomputers, fully three-dimensional Navier-Stokes solvers can't be run with enough grid points or too small enough residuals to eliminate concerns of numerical inaccuracies. The conclusion reached in Ref 16, that an asymmetric disturbance is required to maintain an asymmetric flow, is tainted by the fact that it is based on an underresolved and underconverged 3-D Navier-Stokes computation.

The first Navier-Stokes computations of asymmetric separated flow were done using a center difference finite volume code (Ref 15). The computational procedures used in this code are detailed in Ref 23, 24, and 25. The computation is formally second order in space; it requires a fourth-order added dissipation to avoid odd-even decoupling and second-order dissipation to stabilize the computation near shocks. The present investigation uses a third-order upwind biased scheme similar to that present in Ref 26. The scheme needs no explicitly added dissipation. The odd-even decoupling is eliminated by upwind differencing, and in the cases studied here the shocks were so weak that no shock dissipation was needed. Figure 2 compares results from the centered code (Ref 15) to those of the upwind code. The free-stream conditions are those used as a standard for the rest of this report: 5-deg cone at M_∞ = 1.8 and a Reynolds number based on the distance (R, Fig. 1) from the cone apex, i. e., $R_e = 10^5$. The plot shows side force as a function of angle of attack. The experimental data of Peak (Ref 4) is included for comparison. The two computations compare well up to the maximum in side force (α/δ = 4). Both codes predict the same critical angle of attack (i.e. the angle of attack at which the side force begins to grow from zero). The centered code continues to predict steady flow above this angle of attack while the upwind code predicts unsteady flow. The rapid drop in the experimental side may be due to unsteady vortex shedding. Above α/δ = 4.9, there is no question but that the flow is unsteady experimentally while the centered code predicts steady flow up to α/δ = 5.9. It was noted in Ref 15 that numerical dissipation has a tendency to stabilize unsteady flows. For this reason, the Navier-Stokes computations of the present investigation were performed with the upwind code.

2.1 CORRELATION OF FIRST APPEARANCE OF SADDLE/NODE & CRITICAL ANGLE OF ATTACK

It had been noted experimentally (Ref 4) that the critical angle of attack corresponded closely to the first appearance of a saddle/node combination in the lee symmetry plane of circular cones. The cross-flow streamline pattern of the symmetry imposed solution below and above the angle of attack at which the saddle first appears is shown in Fig. 3a and 3b, respectively. The saddle and node are pointed out in Fig. 3b while only one stagnation point (a node) exist in the stream line pattern of Fig. 3a, it being on the surface of the cone in the lee plane. The stagnation points may be clearer in the lee plane velocity profiles of Fig. 4a and b. The lower stagnation point is the saddle while the upper is the node.

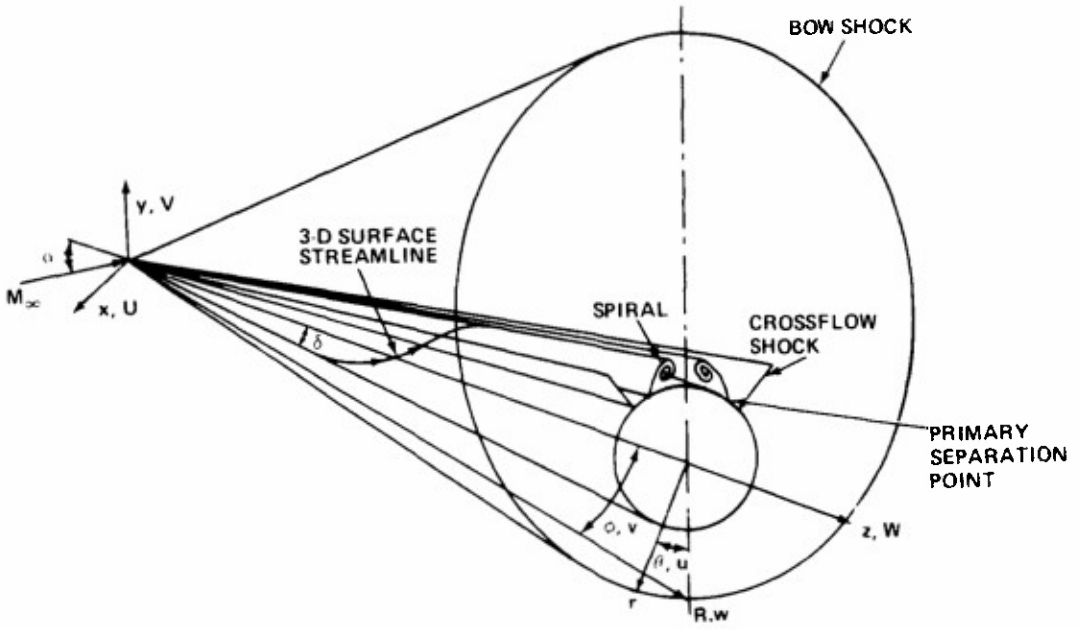

Fig. 1 Sketch of Flow Field & Coordinate System

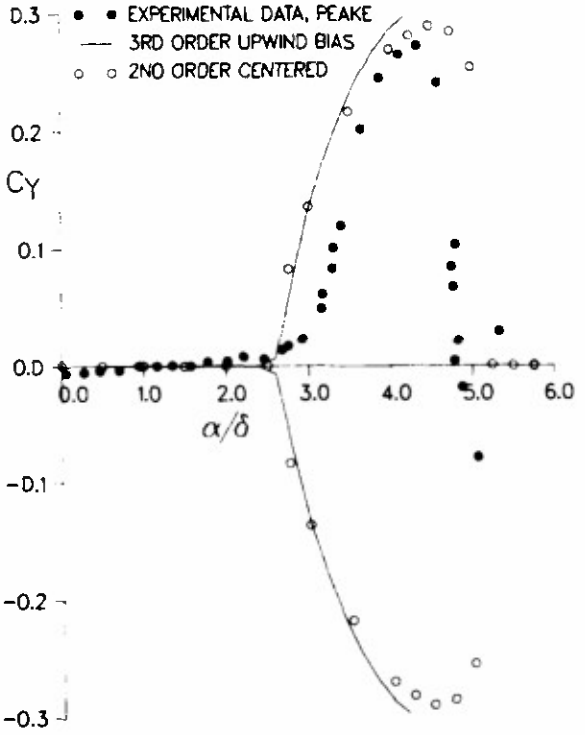

Fig. 2 Computed Side Force Comparison (M_∞ = 1.8, δ = 5°, $R_\theta = 10^5$)

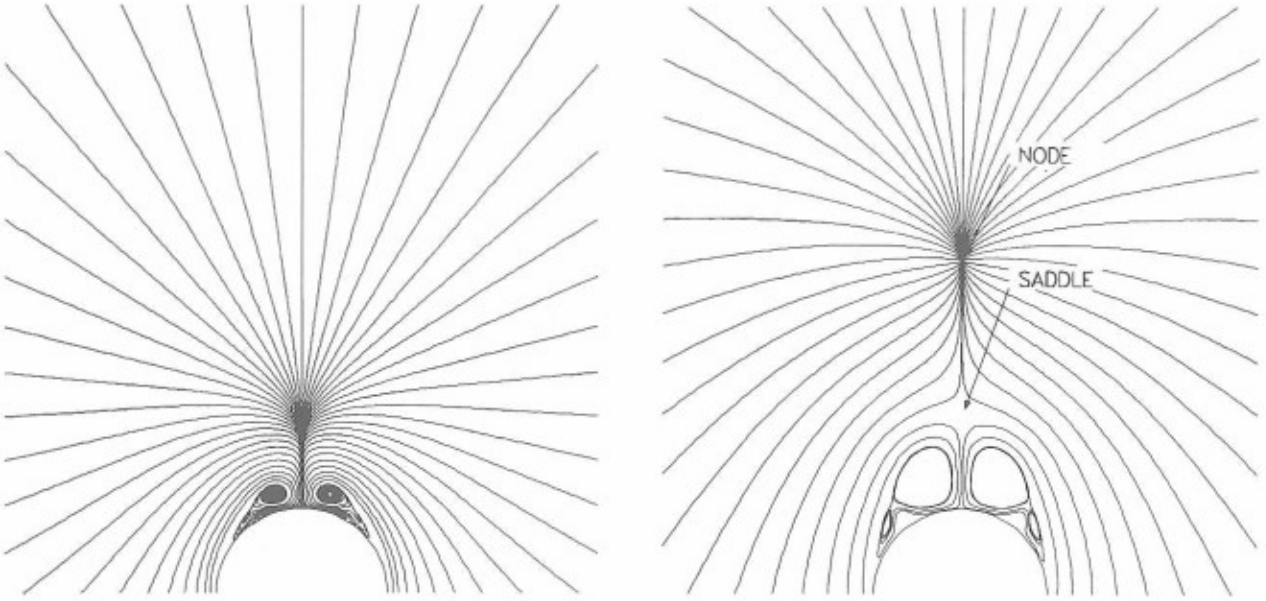

(a) Subcritical (b) Supercritical

Fig. 3 Subcritical & Supercritical Cross-Flow Stream Lines ($M_\infty = 1.8$, $\delta = 5^\circ$, $R_\theta = 10^5$)

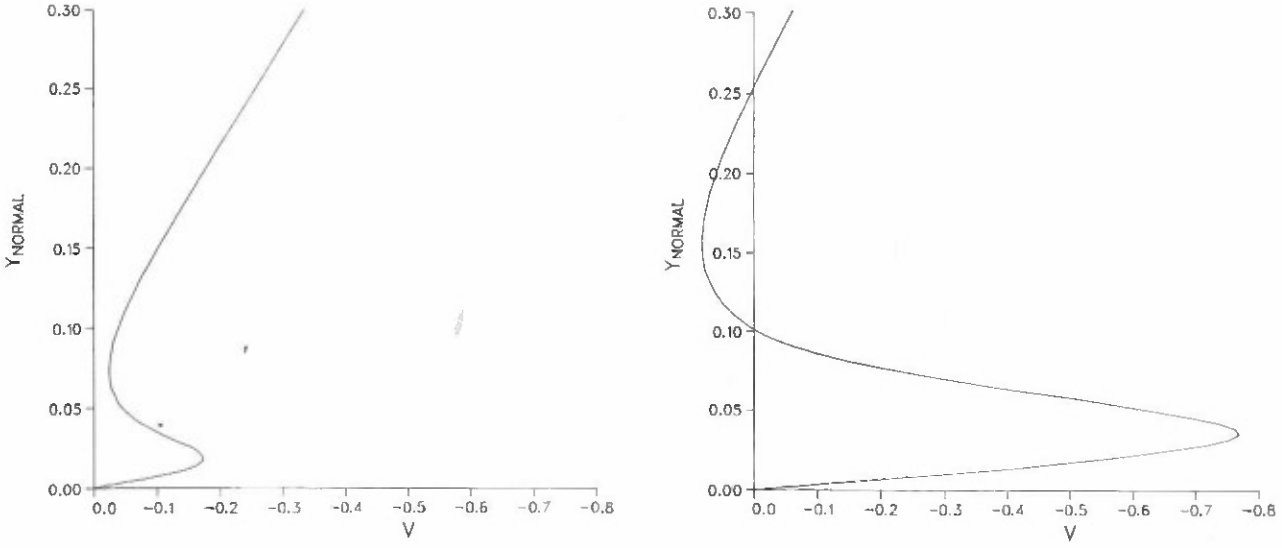

(a) Subcritical (b) Supercritical

Fig. 4 Lee Plane Velocity Profiles ($M_\infty = 1.8$, $\delta = 5^\circ$, $R_\theta = 10^5$)

It is indeed true that for a 5-deg half-angle circular cone at $M_\infty = 1.8$ the critical angle of attack corresponds to the angle of attack at which the saddle/node first appears in the flow field. This was determined by increasing the angle of attack in small increments near the critical angle of attack. In order to determine if the finding was universal, the cross-sectional geometry of the configuration was varied. Figure 5 shows regions of solutions in the angle of attack / cross-sectional eccentricity space. The "one solution" region corresponds to the subcritical flow where only the symmetric solution exists. The "two solutions" correspond to the mirror image asymmetric flows. The "no solution" region corresponds to angles of attack and eccentricities where the iteration scheme used could not converge to a steady solution. It is assumed that the flow is indeed unsteady (i. e., shedding vortices) in this area of the angle of attack eccentricity space. In the case of the circular cone (b/a = 1) the solution follows a simple trend as the angle of angle of attack is increased. Only the symmetric solution exists until the critical angle of attack is reached ($\alpha = 12°$) above which the two asymmetric solution exist until the flow goes unsteady above $\alpha = 22°$. In the case of a vertically elongated ellipse (b/a = 1.8), the solution variation is not as simple. The critical α is 8°, but the flow becomes symmetric again at $\alpha = 16°$ before it goes unsteady at $\alpha = 20°$. Above b/a = 1.9 and below b/a = 0.7, the symmetric flow goes unsteady without passing through a region of asymmetric flow. Also in Fig. 5 is a curve showing the onset of saddle in terms of angle of attack and eccentricity. The onset of the saddle corresponds very closely to the critical angle of attack for eccentricities between 0.9 and 1.6, but outside this range there is a significant difference. It can not be concluded that the saddle is the singular point in the flow which destabilizes the symmetric solution. The phenomenon seems somewhat global and as such can not be attributed to an isolated flow feature.

The interaction of the two vortices near the lee plane is obviously related to the phenomenon of asymmetric separation. The study of the effect of cross-sectional eccentricity summarized in Fig. 5 further substantiates this assumption. As the cross section becomes flatter (lower b/a), the strength of the separation vortices increases, and yet the critical angle of attack goes up as b/a decreases below 1.5. This must be attributed to the fact that the vortices are moving away from each as the cross section approaches a flat plate. On the other hand, while the vortices are very close for vertically elongated ellipses (b/a > 1), the critical angle of attack again goes up for b/a > 1.5 because the vortices are very weak. An attempt was made to quantify this

process, but the difficulty in evaluating the circulation around the numerically computed vortices made this impossible.

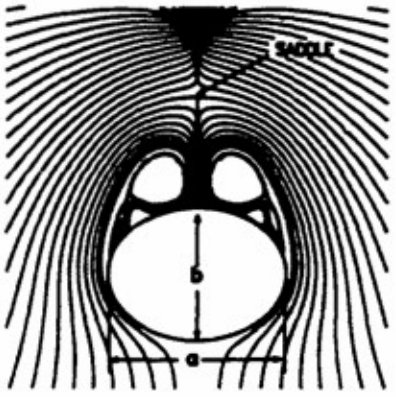

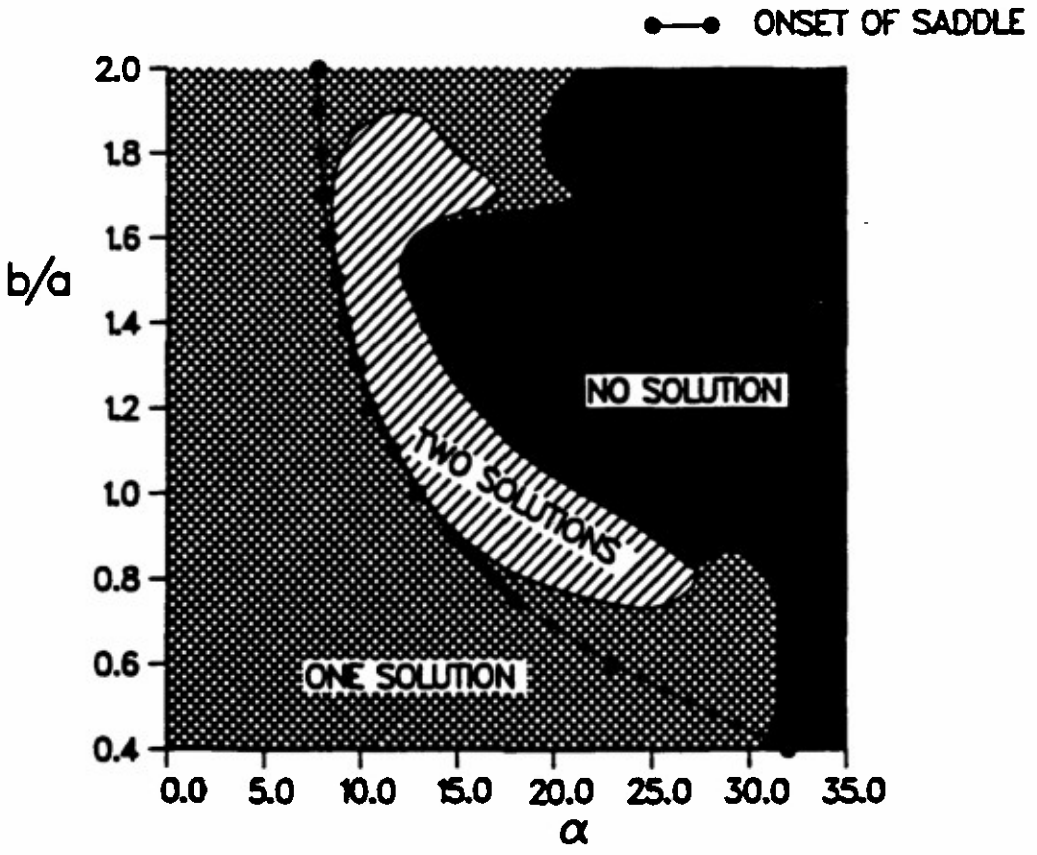

Fig. 5 Comparison of Solution & Saddle Point Existence in Angle of Attack Eccentricity Domain ($M_\infty = 1.8$, $\delta = 5^\circ$, $R_e = 10^5$)

2.2 REGIONAL ISOLATION OF ASYMMETRY

This aspect of the investigation involved trying to pinpoint the instability in the symmetric flow above the critical angle of attack by isolating regions of the flow. The symmetric solution was generated by imposing symmetry on the calculation and continuing until machine zero was reached. With the symmetric solution as initial conditions, only portions of the flow were computed with the symmetry condition removed. In addition, an asymmetric disturbance was injected in the computed portion of the flow. The hope was that if the computed region of the flow included the unstable point the computation would not converge, while if the singular point was not surrounded the computation would converge to the original symmetric solution. Consider Fig. 6 in which a region of the flow surrounding the vortices is bounded by a dashed line. The flow field shown is that computed by imposing symmetry. A computation is started with this symmetric solution used as initial conditions. Moreover, the flow field outside the dashed box is held fixed at these symmetric conditions. The flow conditions inside the box are asymmetrically perturbed, and the computation is continued. The hope was that if the box did not include any unstable flow features, the computation would converge to the symmetric result since essential symmetry was being imposed in the unstable portion of the flow, and only the stable portion was allowed to be asymmetric. This is true of the region in the dashed box shown in Fig. 7. The region is far from the vortices and is benign. On the other hand, no convergence is achieved in the computation when the region shown in Fig. 6 is allowed to change (and is indeed asymmetrically perturbed.). It seems obvious that in the case of the region inside the box of Fig. 6, the computed portion of the flow is unstable, and the symmetric boundary conditions on the dashed line are incompatible with what the flow inside the box wants to converge to. With these encouraging results, the computed region (i. e., the box of Fig. 6) was shrunk to try to further isolate the unstable portion of the flow field. This is the point where the technique failed. As long as the vortex centers were encompassed, the computation would not converge. If the region computed was too small to encompass the vortices, convergence would be reached. For example, the computation of the region shown in Fig. 8 converged to the symmetric result.

This finding indicated again that the instability was of a somewhat global nature. At a very minimum, the vortices had to be included in order for the instability to exhibit itself. It seems to be the interaction of the vortices, in a global sense, and

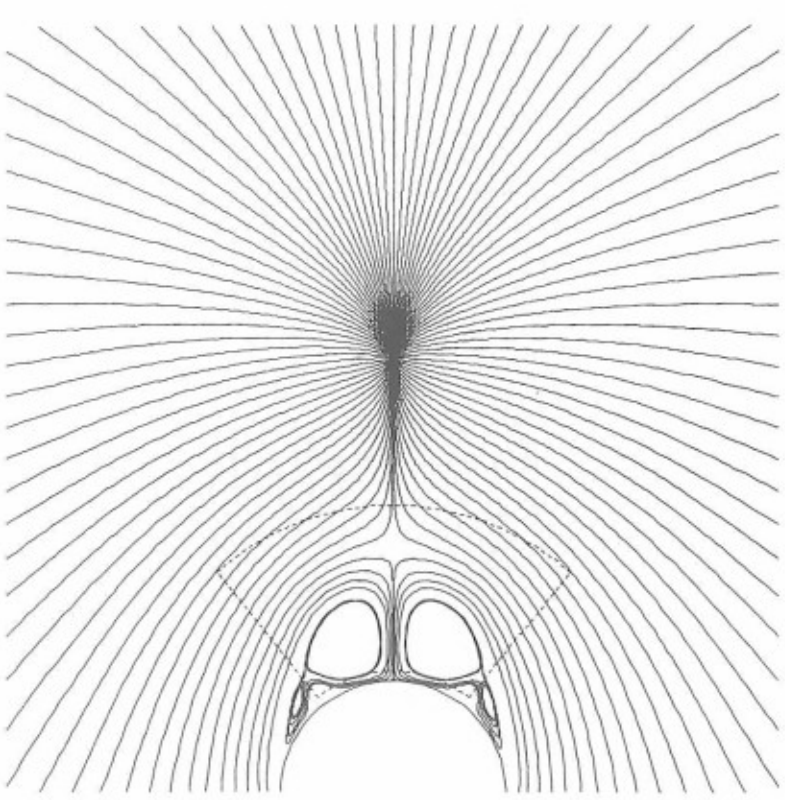

Fig. 6 Isolation Study, Region Containing Vorticea – No Convergence
($M_\infty = 1.8, \delta = 5°, \alpha = 20°, R_e = 10^5$)

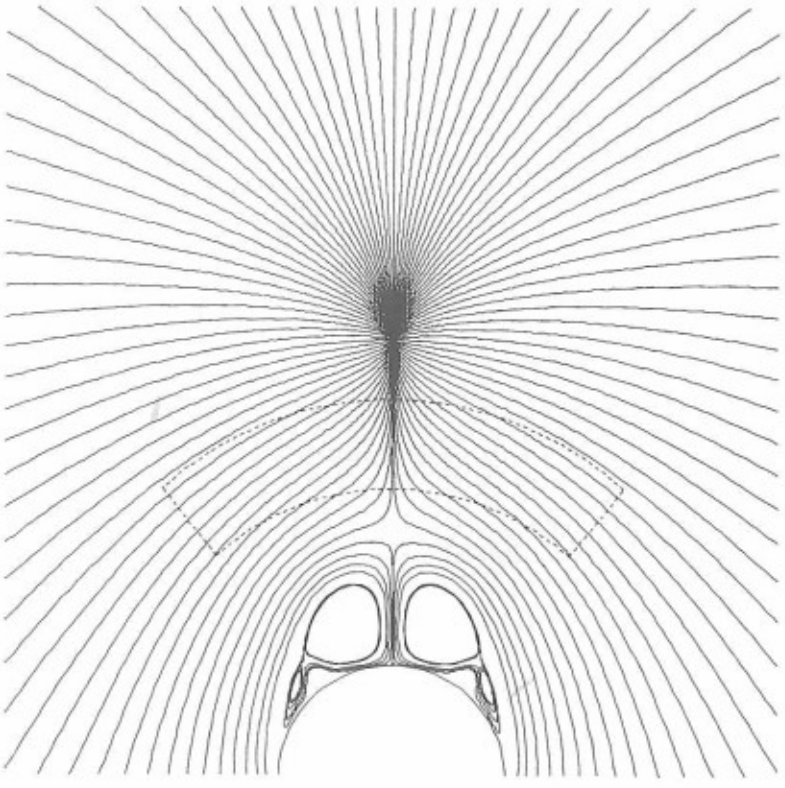

Fig. 7 Isolation Study, Benign Region – Convergence
($M_\infty = 1.8, \delta = 5°, \alpha = 20°, R_e = 10^5$)

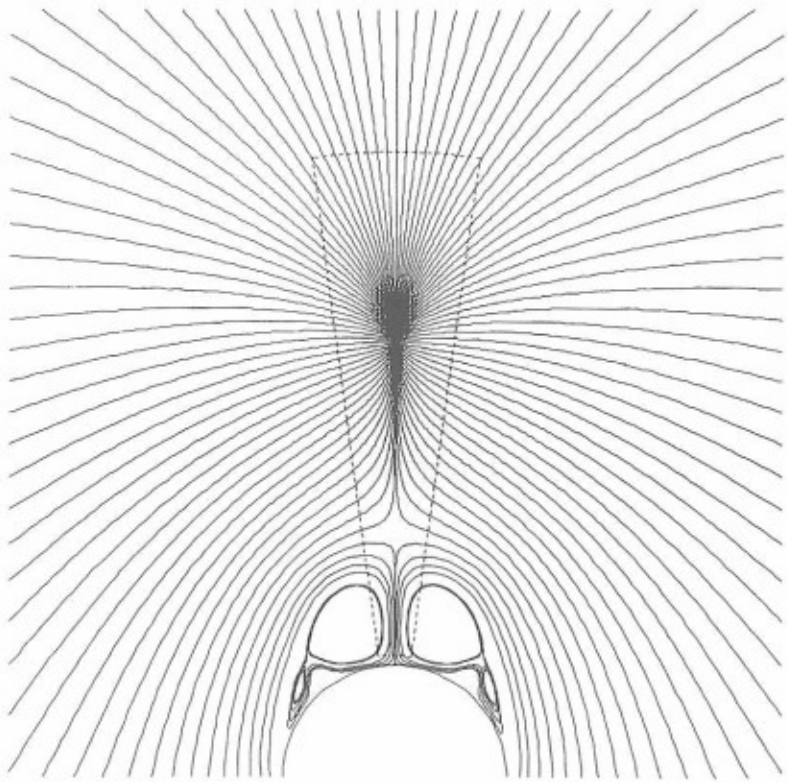

Fig. 8 Isolation Study, Region Near Symmetry Plane – Convergence
($M_\infty = 1.8$, $\delta = 5°$, $\alpha = 20°$, $R_\theta = 10^5$)

not a singular point in the symmetry plane which is the cause of the instability in the symmetric solution. This instability in turn results in the asymmetric flow.

2.3 LOCAL STABILITY ANALYSIS

The local stability analysis considered here is based on an Orr-Sommerfeld type procedure. First, the viscous terms in the governing equations are neglected. It has been shown in Ref 7 and 14 that the phenomenon of asymmetric separation is inherently inviscid. The instability in the symmetric solution appears at the critical angle of attack without the viscous terms included in the governing equations of Ref 7 and 14. The results presented therein prove that not only is the phenomenon inviscid, but it is also governed by the conical flow equations. The stability analysis considered here starts from the conical continuity and the following Euler equations:

$$\rho_t + 2\rho w/R + (\rho u \sin\theta)_\theta/R \sin\theta + (\rho v)_\phi/R \sin\theta = 0$$

$$u_t + uu_\theta/R + vu_\phi/R \sin\theta + wu/R - v^2 \cot\theta/R = -p_\theta/\gamma r R$$

$$v_t + uv_\theta/R + vv_\phi/R \sin\theta + wv/R - uv \cot\theta/R = -p_\phi/\gamma r R \sin\theta$$

$$w_t + uw_\theta/R + vw_\phi/R \sin\theta - (u^2+v^2)/R = 0$$

The conical coordinates R, ϕ and θ and velocity components u, v and w are defined in Fig. 1, and ρ and p are the density and pressure. All independent variables are then assumed to be the sum of a "base flow field" (ρ,U,V,W) and a small perturbation (ρ',u',v',w'). It is the stability of the numerically generated symmetric solution being investigated here so that this is the base flow field used. All variations in entropy are third order in the perturbation's quantities so that they are negligible. The equation of state becomes $p = \rho^\gamma$ so that the pressure derivative p_ϕ in the above equations can be replaced by $\gamma\rho^{\gamma-1}\rho'_\phi$ (p_θ is replaced similarly). After substituting in terms of the perturbation variables and neglecting all second-order terms in the perturbation quantities, and while remembering that the base solution satisfies the governing equations, a linear system of equations is arrived at:

$$\rho'_t + 2(\rho'W+w'\rho)/R + [(\rho'U + u'\rho)\sin\theta]_\theta/R \sin\theta + (\rho'V + \rho v')_\phi/R \sin\theta = 0$$

$$u'_t + (Uu' + u'U)_\theta/R + (Vu' + v'U)_\phi/R\sin\theta + (Wu' + w'U)/R - 2v'V\cot\theta/R = -\rho'_\theta\rho^{\gamma-2}/R$$

$$v'_t + (Uv' + u'V)_\theta/R + (Vv')_\phi/R\sin\theta + (Wv' + w'V)/R + (Uv' + u'V)\cot\theta/R = -\rho_\phi\rho^{\gamma-2}/R\sin\theta$$

$$w'_t + (Uw' + u'W)_\theta/R + (Vw' + Wv')_\phi/R\sin\theta - 2(Uu'+Vv')/R = 0$$

At this point the form of the unsteady oscillation is assumed:

$$\rho' = \rho''(\phi)\, e^{i(\beta\theta-\omega t)}$$

$$u' = u''(\phi)\, e^{i(\beta\theta-\omega t)}$$

$$v' = v''(\phi)\, e^{i(\beta\theta-\omega t)}$$

$$w' = w''(\phi)\, e^{i(\beta\theta-\omega t)}$$

Here β is real and is related to the wavelength of the disturbance (the wavelength $\lambda = 2\pi/\beta$). The quantity ω is complex, with its real part being the frequency of the oscillation and its imaginary part the amplification factor. The amplitude functions (ρ'',u'',v'',w'') are all considered functions only of ϕ in this form of the disturbance. An oscillation of the form $\mathbf{f}'=\mathbf{f}''(\theta)\, e^{i(\beta\phi-\omega t)}$ ($\mathbf{f}=\{\rho,u,v,w\}$) was also considered. After substituting into the linear governing equations, a system of linear, homogeneous ODEs results. The perturbations to the base flow are assumed to vanish at the boundaries of the computational domain, making the boundary conditions of the linear problem homogeneous. The resulting mathematical problem is a two-point boundary value problem for the system of equations:

$$\mathbf{A}\, d\mathbf{f}''/d\phi + \mathbf{B}\,\mathbf{f}'' - i\,\omega\,\mathbf{f}'' = 0$$

where $\mathbf{f}'' = \{\rho'',u'',v'',w''\}$ and **A** and **B** are 4x4 coefficient matrices made up of the given base flow field. **A** and **B** are also functions of the wavelength parameter β. The boundary conditions on the perturbation vector $\mathbf{f}''$ are $\mathbf{f}'' = 0$ at both $\phi = \phi_{body}$ and $\phi = \phi_{far\ field}$. The boundary value problem has a non-trivial solution (i. e., non-zero eigenvectors $\mathbf{f}''$) for only certain value of ω; these are the eigenvalues of the problem.

These are computed for all possible wavelengths. If any eigenvalue has a positive imaginary part for a disturbance of a particular wavelength, the base flow is unstable to that disturbance.

This procedure follows the classical Orr-Somerfeld local stability analysis (Ref 27). It has been used successfully to investigate the stability of given velocity profiles in the study of transition from laminar to turbulent flow. It is this type of stability analysis which predicts that it is inflection points in velocity profiles that are the source of the instability in boundary layer type flows. This same procedure was used successfully to study the stability of numerical solutions for the flow in the wake of cylinders and flat plates (Ref 28-29). The inviscid Orr-Somerfeld boundary value problem is defined by the ODE:

$$(U - \omega/\beta)\,(d^2\psi/dy^2 - \beta^2\psi) - d^2U/dy^2\,\psi = 0$$

with boundary conditions $\psi = 0$ at $y = 0$ and $y = \infty$. The system of equations (continuity and two momenta) is reduced to a single equation by using stream function formulation. Here ψ is the amplitude function associated with the perturbation of the stream function (ψ is the eigenvalue of the boundary value problem) and U is the base velocity profile. Given a velocity profile, its stability is determined by computing all eigenvalues (ω) for each wavelength parameter (β). If the eigenvalues have any positive imaginary part, the velocity profile is unstable.

The numerical procedure for solving the eigenvalue problem is relatively straightforward. If the inviscid Orr-Somerfeld equations are discretized using a centered difference scheme, a system of equations of the following form results:

$$(U_i - \omega/\beta)\,\{(\psi_{i+1} - 2\psi_i + \psi_{i-1})/\Delta y^2 - \beta^2\psi_i\} - (d^2U/dy^2)_i\,\psi_i = 0$$

or in matrix form:

$$\mathbf{a}\,\psi + \omega\,\mathbf{b}\,\psi = 0$$

where now ψ is the vector $\{\psi_1, \psi_2, \psi_3, \ldots \psi_{imax}\}$ of length imax (the number of grid points considered) and **a** and **b** are the tridiagonal coefficient matrices. If this equation is simply rearranged into the form

$[\mathbf{b}^{-1}\,\mathbf{a}]\,\psi + \omega\,\psi = 0,$

the problem is reduced to finding the eigenvalues and eigenvectors of a matrix $\mathbf{c} = \mathbf{b}^{-1}\,\mathbf{a}$. This is done directly with computer library routines. In the present work the computer library routines EVCCG and EVLCG were used; these were obtained from the IMSL library (Ref 30) which is available on Grumman's Cray YMP. In this way imax-2 (because the two boundary points are eliminated) eigenvalues of ω are determined.

In order to check the accuracy of the scheme used to compute the eigenvalues, a boundary value problem with an analytical solution was considered. The classical "rotating string" problem was chosen:

$d^2y/dx^2 + \omega y = 0$

$y(0) = 0$ and $y(1) = 0$.

The exact eigenvalue corresponding to the m^{th} mode for this problem is $\omega_m = m^2\,\pi^2$. With the corresponding eigenvalues, $y_m = C\,\sin(m\pi x)$ where C is an arbitrary constant. The finite difference form of the rotating string ODE is:

$(y_{i+1} - 2\,y_i + y_{i-1})/\Delta x^2 + \omega\,y_i = 0$

For this simple problem the matrix **b** is the identity matrix ($b_{ii} = 1$ and $b_{ij} = 0$ for $i \neq j$). The matrix **a** is simply the second derivative tridiagonal matrix ($a_{ii} = -2/\Delta x^2$, $a_{ii-1} = a_{ii+1} = 1/\Delta x^2$ and all other $a_{ij} = 0$). Figure 9 compares results of computations using three different grids to solve the rotating string problem. The figure is a plot of eigenvalues normalized with respect to its exact value vs mode. It is clear that only with the very fine grid (400 points) are the higher modes computed accurately. This result indicated that a more accurate scheme was required. In stability analyses, spectral methods are popular because of their increased accuracy over finite difference methods. The procedure starts by assuming a truncated Fourier series for the eigenvectors $y = \sum Y_i \sin(i\pi x)$. The sum is over i=1 to imax. The sine series is chosen so that the boundary conditions ($y(0) = y(1) = 0$) are automatically satisfied. After substitution, the rotating string ODE becomes:

$-\sum i^2\pi^2 Y_i \sin(i\pi x) + \omega \sum Y_i \sin(i\pi x) = 0.$

The equation must be satisfied at (imax-2) points in order to solve for the (imax-2) coefficients Y_i. (The two end points are omitted since the boundary conditions are automatically satisfied.) This leads to a system of linear equations similar to that arrived at with the finite difference scheme. The matrices **a** and **b** are now full and not tridiagonal:

$a_{ij} = -j^2\pi^2 \sin(j\pi x_i)$

$b_{ij} = \sin(j\pi x_i)$

The library routines EVCCG and EVLCG (Ref 30) can find the eigenvalues and eigenvectors of full matrices as well as tridiagonals. The spectral method gives the exact solution to the string problem independent of how many point terms of the series are retained. This test is somewhat unfair since the sine series is the exact solution in this case.

The next problem on which the method was tested was the inviscid Orr-Sommerfeld problem. The stability of two velocity profiles U(y) was considered. Figure 10 shows both a stable and an unstable velocity profile. The stable velocity profile is attached. In addition, the stable profile has no inflection points. All the eigenvalues ω are real (i. e., have zero imaginary parts) for this profile. All values of the wavelength parameter β were interrogated. On the other hand, when the separated profile of Fig. 10 was considered, unstable eigenvalues were found. Figure 11 shows the maximum imaginary part of the eigenvalues ω as a function of wavelength parameter β from 0 to π. The unstable velocity profile of Fig. 10 is unstable to disturbances for $\beta < 2.8$ and stable to disturbances with larger values of β (i. e., smaller wavelengths). Also shown in Fig. 11 is a comparison of the eigenvalues computed with the finite difference scheme (200 points) and the spectral method (200 term series). This comparison shows that the advantage of using the spectral method is lost in the case of the inviscid Orr-Sommerfeld problem. Finally, Fig. 12 compares the computed real part of the eigenvector corresponding to the maximum eigenvalue ($Im(\omega) = 0.224$) for $\beta = 0$. Again this comparison shows little advantage of the spectral method.

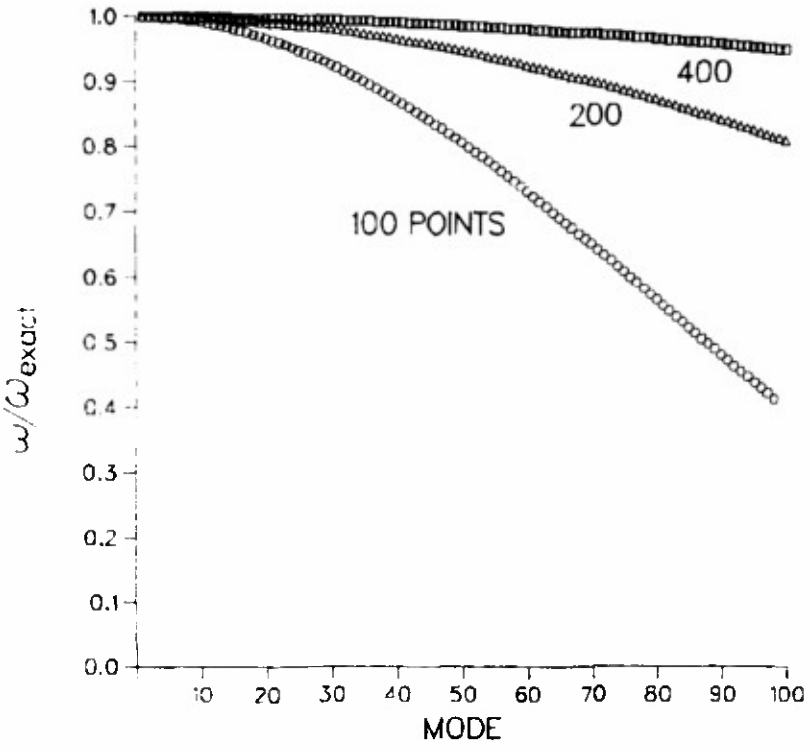

Fig. 9 Comparison of Computed Eigenvalues Rotating String Problem

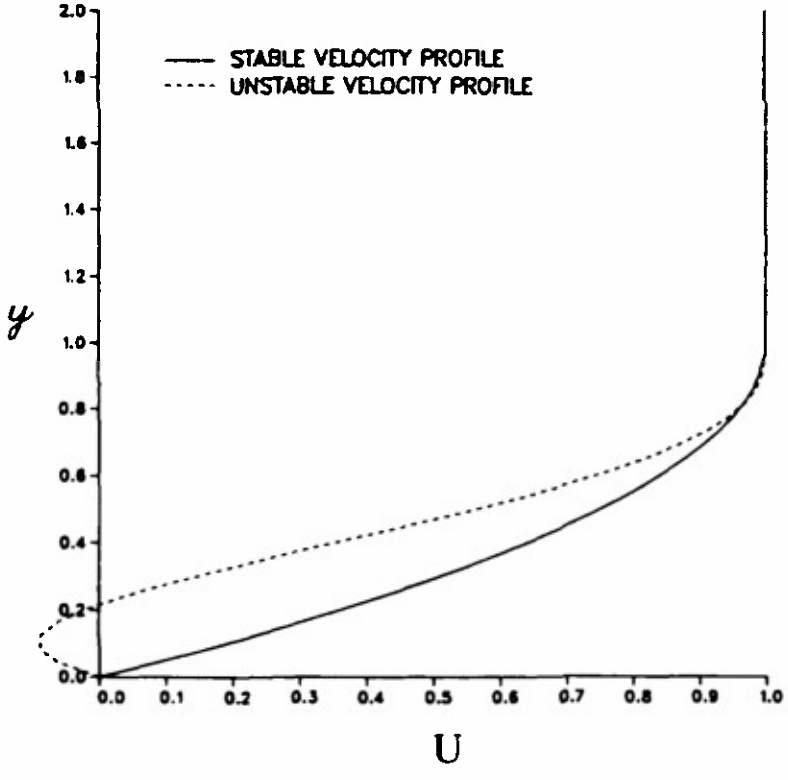

Fig. 10 Stable & Unstable Velocity Profiles

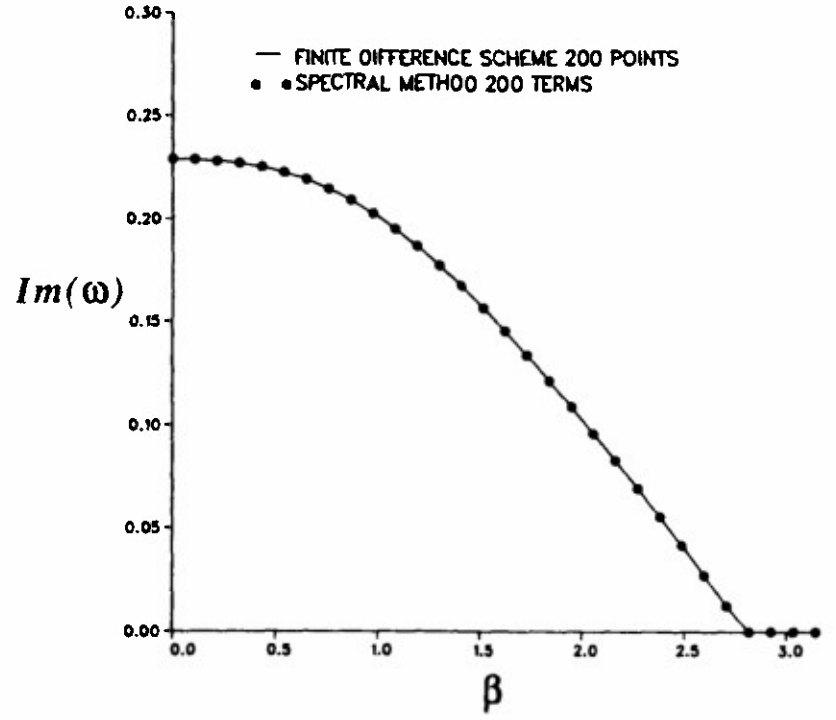

Fig. 11 Comparison of Computed Eigenvalues Orr-Sommerfeld Equation. Separated Velocity Profile

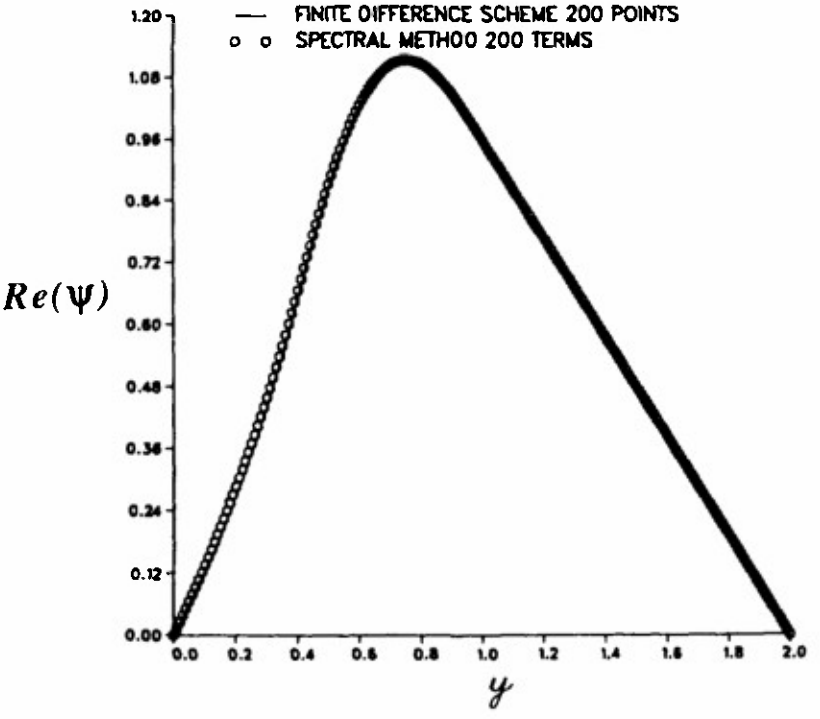

Fig. 12 Comparison of Computed Eigenvectors Orr-Sommerfeld Equation, Separated Velocity Profile

The spectral method was applied directly to the system of conical equations,

$$\mathbf{A}\, d\mathbf{f}''/d\phi + \mathbf{B}\, \mathbf{f}'' - i\,\omega\, \mathbf{f}'' = 0,$$

in an effort to determine the stability of the supercritical flow computed by imposing symmetry. A Fourier sine series of the form $\Sigma\, F''_i \sin(i\pi\phi)$ is assumed for the vector $\mathbf{f}''$. The 4x4 system of ODEs is satisfied at imax-2 points in the flow field. These points are in a cross-flow plane (the flow is always assumed conical) but in addition the are also on a ray θ = a constant (see Fig. 1). The Orr-Sommerfeld stability analysis in one-dimensional in nature. As in the case of the inviscid Orr-Sommerfeld equation the matrices **a** and **b** are formed and the resulting linear system becomes:

$$\mathbf{a}\,\mathbf{F} + \omega\,\mathbf{b}\,\mathbf{F} = 0.$$

Now the vector **F** is 4 elements for each imax-2 points in the flow field. The matrices **a** and **b** are 4x4x(imax-2)x(imax-2). Even with these large matrices, the Cray was able to evaluate their eigenvalues very quickly.

The results of the analysis were somewhat disappointing. The problem seems to be imbedded in the assumption of the form of the disturbance. The analysis always predicts unstable flow, even if low angles of attack are considered. This is obviously incorrect; the numerical scheme is able to compute stable flow fields below the critical angle of attack. The result predicted by the stability must be due to the assumptions made during its development. The Orr-Sommerfeld analysis has been used successfully to study the stability of boundary layer type flows (Ref 27) where the variations in flow variables in the main flow direction are small. This is not true in the cross-flows considered here. The roles of the two cross-flow plane coordinates were reversed in the disturbance (*i. e.*, $\mathbf{f}'=\mathbf{f}''(\theta)\, e^{i\,(\beta\phi-\omega t)}$) to no avail. All flows have some positive Im(w) for some range of wavelength parameter β. This result implies that the phenomenon is fully two-dimensional and that the cause of the instability may not be attributable to a singular point such as an inflection point in a boundary layer profile. It is clear that the interaction that results in the instability considered here is somewhat global in nature.

2.4 TRANSITION OF THE FLOW FROM THE SYMMETRIC SOLUTION

This investigation was carried out by starting a Navier-Stokes solver with a symmetric solution and very carefully monitoring the transition to the asymmetric flow. The supercritical symmetric solution was generated by imposing symmetry (half-plane calculation). The development of the asymmetric solution was monitored by computing the difference between the components of the solution vector at left and right image points. Those components that should be symmetric are differenced and the one which is anti-symmetric is added. The solution vector **Q** has five components $\{\rho,\rho U,\rho V,\rho W,E\}$. The components $\rho,\rho U,\rho W$ and E should be symmetric while ρV should be anti-symmetric. Let $\delta\mathbf{Q} \equiv \{\rho_L-\rho_R,(\rho U)_L-(\rho U)_R,(\rho V)_L+(\rho V)_R,(\rho W)_L-(\rho W)_R,E_L-E_R\}$ at each point in the flow field. At every step of the iteration, $\delta\mathbf{Q}$ is monitored. Figure 13 shows the maximum asymmetry (δQ) and the maximum residual (RES) as a function of iteration step. The maximums, both δQ and RES, are the maximums of the five components of the vectors **dQ** and **RES** at each grid point and in turn the maximum over all grid points in the flow field. The free-stream conditions for the iteration history shown in Fig. 13 are supercirtical (5-deg cone at $\alpha = 20°$ and $M_\infty = 1.8$) while the initial flow field was computed using the symmetry condition.

The forced symmetric initial conditions result in a maximum δQ of 10^{-12} and a maximum RES of 10^{-14} after the first step of the unforced (full-plane) iteration. The initial conditions in the unforced calculation are generated by reflection of the symmetric solution, resulting in a δQ of absolute zero. The asymmetry becomes 10^{-12} after the first step of the unforced calculation because this is machine zero for this quantity for the scheme used here. This is the smallest value of δQ achievable. If a subcritical case is considered (for example, $\alpha = 10°$) δQ is 10^{-12} at the converged solution. The RES is 10^{-14} because the symmetric iteration was continued until the residual reached that level (machine zero for this quantity).

It is interesting to note the way in which both these quantities grow from their initial values in Fig. 13. The asymmetry δQ grows from the beginning of the unforced calculation. This is to be expected since the forced symmetric solution is indeed unstable. On the other hand, the residual stays at 10^{-14} for the first 225 steps of the iteration; this is somewhat confusing. Why doesn't the residual grow from the beginning of the iteration as does the asymmetry? It must be remembered, the iteration scheme is designed to force the residual to machine zero and to keep it there

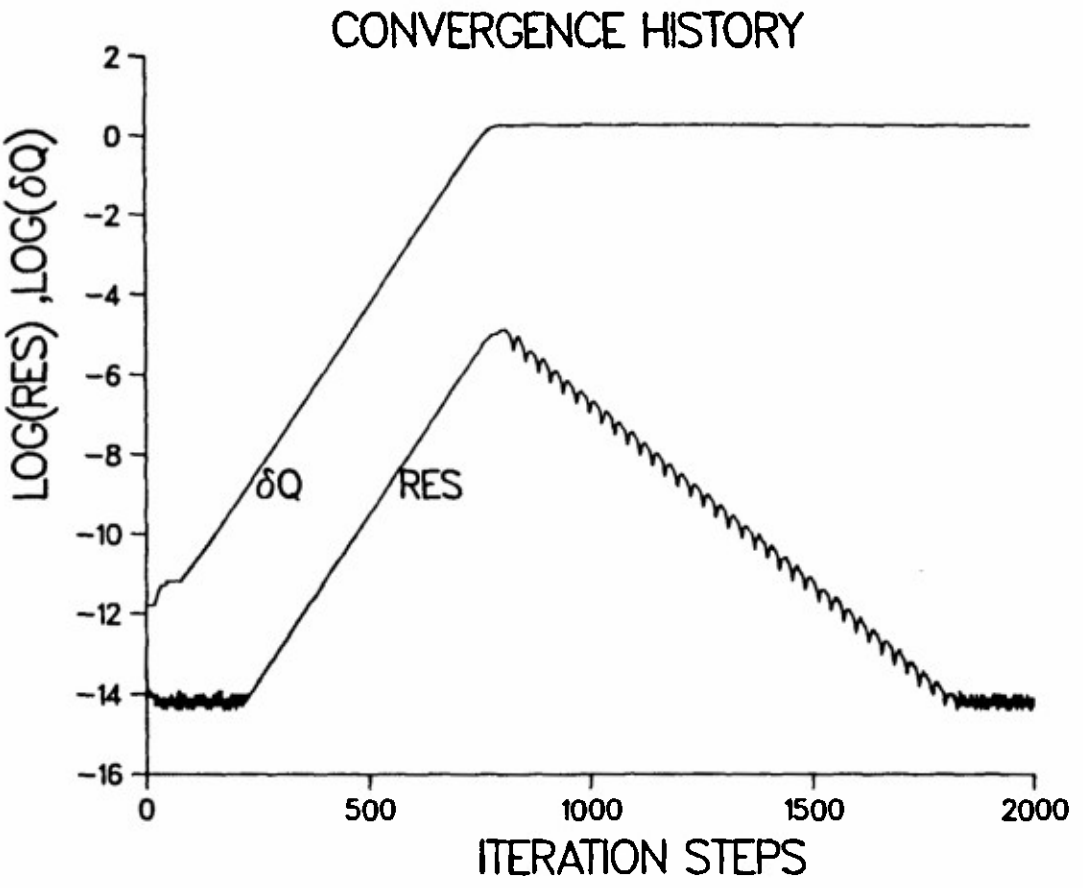

Fig. 13 Convergence History & Development of Asymmetry
($M_\infty = 1.8$, $\delta = 5^\circ$, $\alpha = 20^\circ$, $R_e = 10^5$)

once it arrives. The symmetric solution is a solution to the differential equations, unstable, but yet a solution. With the symmetric flow assumed, the residual is machine zero. The iteration scheme is able to predict corrections to the solution which keep the residual at 10^{-14} until the asymmetric disturbance gets too large (10^{-9}). Once the asymmetric disturbance is large enough, the iteration scheme predicts asymmetric corrections large enough to move the solution toward the asymmetric stable solution. The stable asymmetric solution is essentially established at 800 iteration steps. It should be noted that δQ does not change after 800 steps. Machine zero is arrived at after about 1800 steps, where the stable asymmetric is firmly established. The convergence history of Fig. 13 is typical of a nonlinear problem with two solutions, one stable and the other unstable. With no asymmetric disturbance induced, the iteration scheme will tend toward the symmetric solution, the calculation being inherently symmetric. Once the natural asymmetry, due to machine roundoff, get significant enough to impact the iteration scheme, the asymmetric solution will be approached. The iteration scheme will tend toward the closest solution whether or not it is stable; the iteration scheme is unable to maintain an unstable solution as long as it allows any level of asymmetry. Another interesting aspect of Fig. 13 is the exponential growth of both RES and δQ (the plot is of $\log_{10}$\{RES and δQ\}. The growth rate for both is a constant 0.017. It should be pointed out that the iteration scheme used here is not time accurate so that this growth has no physical meaning.

The development of the flow shown in Fig. 13 was studied in detail using a computer animation technique presented in Ref 31. The transition of the vortex pattern from symmetric to asymmetric is shown clearly in the selected frames of the animation in Fig. 14. The color shading corresponds to entropy, which shows the transition of the vortices very clearly. Figure 14 shows the first 1000 steps of the iteration in increments of just over 15 steps between frames they are arranged matrix form with increasing steps along rows. The flow seems symmetric for a large part of the iteration until frame (6,5) when the asymmetry seems to develop quickly (this corresponds to step 800 of the iteration in Fig. 13). It is very difficult to determine where the asymmetry first appears in an animation made up of frames such as those presented in Fig. 14.

An animation of the root mean square of the vector $\delta \mathbf{Q}$ (i. e., $|\delta \mathbf{Q}|$) does shed some light on the transition to the asymmetric solution from the symmetric one. Figure 15 shows selected frames of an animation in which the color shading corresponds to

$\log_{10}\{|\delta Q|\}$ at each point in the flow field. It should be noted that $|\delta Q|$ is symmetric because it is a difference of right-left or left-right image points. Figure 15 shows the first 200 steps of the iteration with an increment of just over 3 steps between frames. The evolution of $|\delta Q|$ is cyclic. This can be seen by comparing rows 4, 5, 6 and 7 of Fig. 15. At the beginning of the iteration, $|\delta Q|$ is essentially machine zero so that the initial frames of Fig. 15 show no structure (see row 1). As the iteration proceeds, $|\delta Q|$ grows and a structure becomes apparent. This structure is most clearly shown in row 5 of Fig. 15. The asymmetry starts at the edge of the rolled up vortex sheet. It progresses both inward toward the vortex center and outward into the flow field. Note the dark blue color which first appears in frame (5,1) of Fig. 15 and finally dominates a large region around the vortices in last frame of Fig. 15 (7,9). It is clear from the animation of $|\delta Q|$ that the transition from symmetric to asymmetric flow originates in the region of the lee vortices. It is also quite clear that the phenomenon is somewhat global in that the asymmetry does not seem to originate from a point in the flow field but instead starts simultaneously throughout an annulus surrounding the vortex centers. This result, combined with the results presented in the three previous sections of this report, proves that the instability in the symmetric flow above the critical angle of attack, which leads to asymmetric flow, is concentrated in the vortex region but can not be isolated any further.

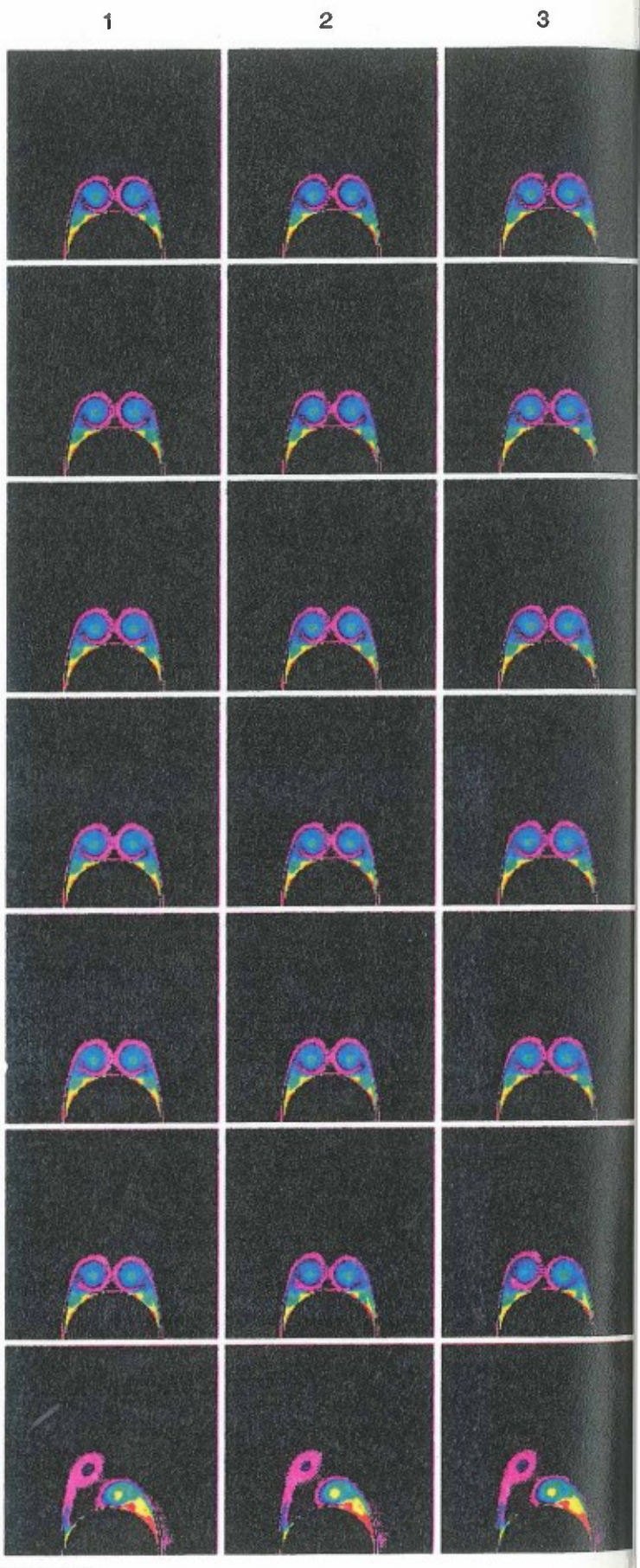

MR92-0789-002

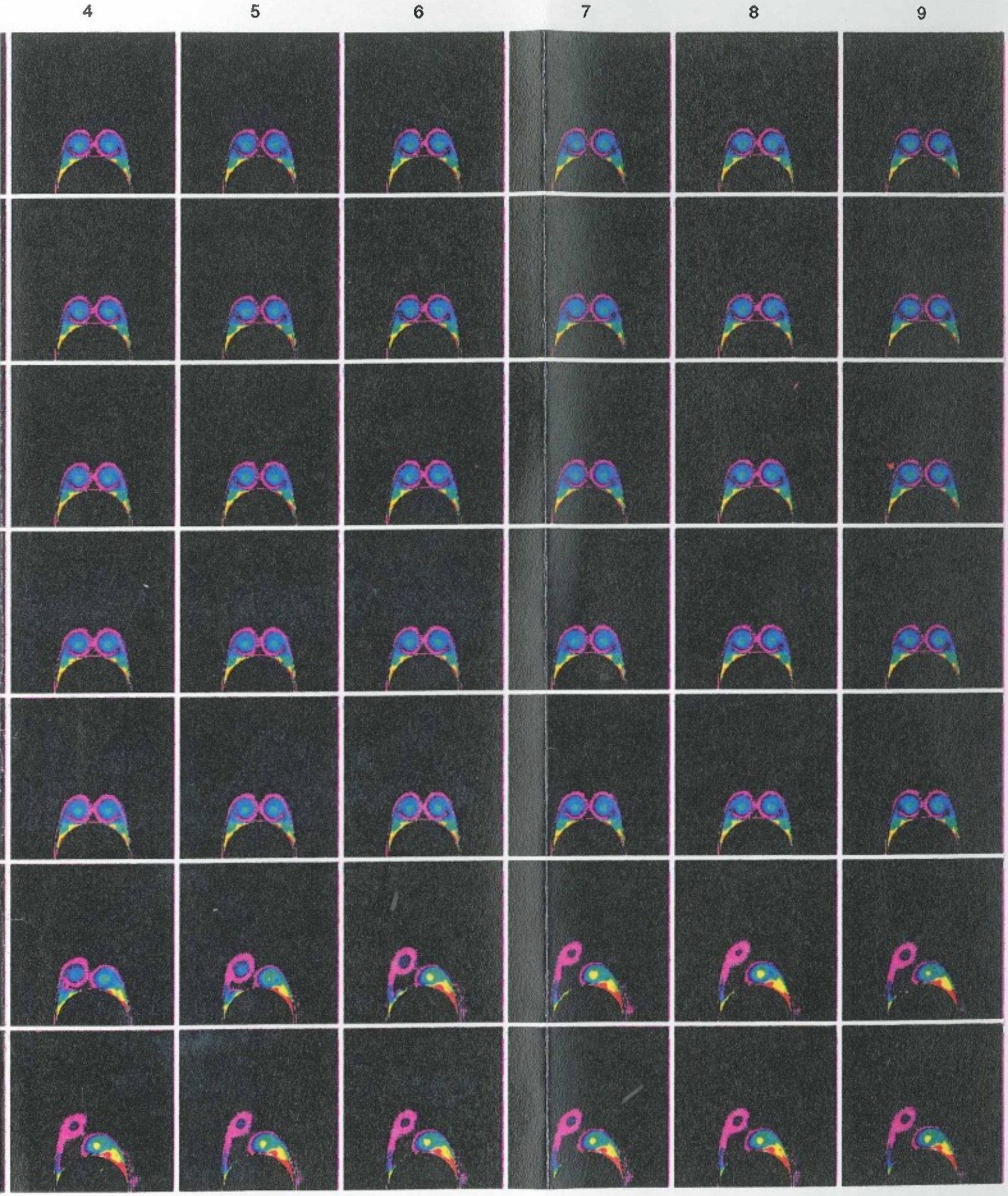

Fig. 14 Selected Frames of Entropy Animation
($M_\infty = 1.8$, $\delta = 5°$, $\alpha = 20°$, $R_e = 10^5$)

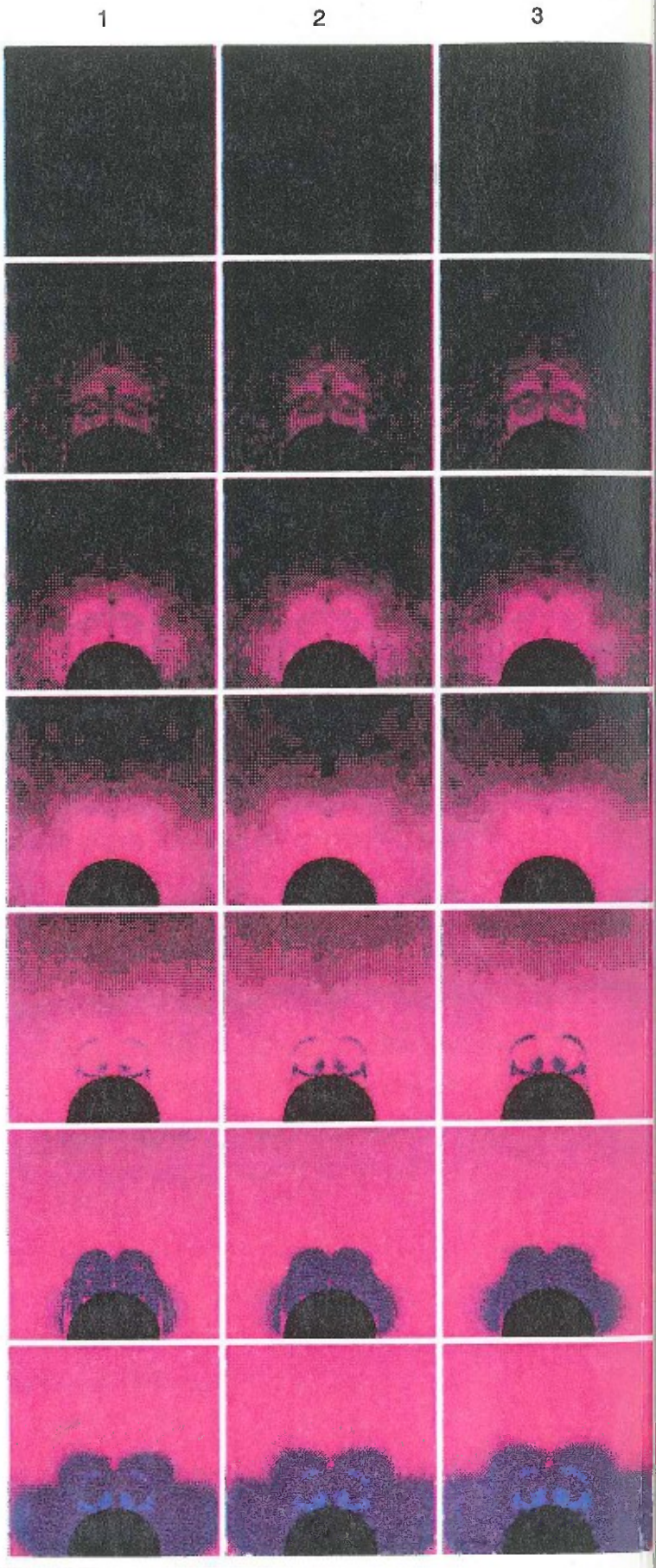

MR92-0789-001

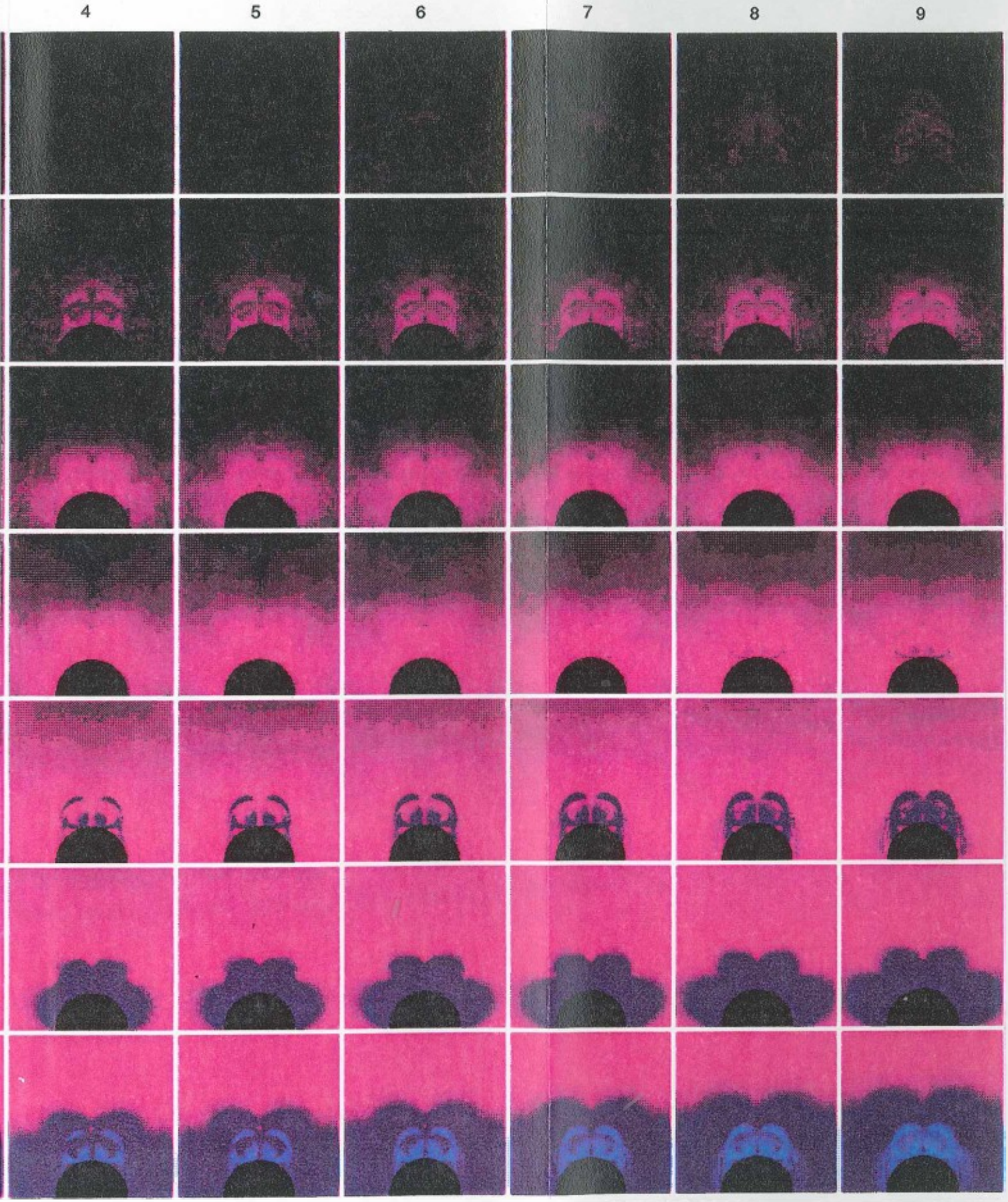

Fig. 15 Selected Frames of Asymmetry Animation
($M_\infty = 1.8$, $\delta = 5^\circ$, $\alpha = 20^\circ$, $R_e = 10^5$)

3. CONCLUSIONS & FUTURE WORK

All of the data generated and analyzed in the present investigation point to the conclusion that the cause of asymmetric separated flow on slender-nosed vehicles at high angle of attack is the interaction of the vortices near the lee plane. This interaction is somewhat global and as such the instability in the symmetric flow (which leads to the asymmetry) can not be traced to any particular flow feature. The likelihood of the phenomenon occuring depends on a quantitative measure of this vortex interaction. The present study indicates that the distance between the vortex centers and the circulation around the vortices are two parameters which play a significant role in the phenomena. Limiting the interaction of the vortices by placing obstacles between them has been known to reduce the side force caused by this phenomenon for many years. Increasing the strength of either or both of the vortices tends to increase the asymmetry, while separating the vortices tends to decrease the asymmetry. From a heuristic point of view, it seems that the mechanism which triggers the asymmetric phenomenon is the two vortices "rolling over" one another. The vortices could be likened to two cylinders touching each other and rotating in opposite directions. If their axes of rotation were allowed to move, their stable position may not have the line connecting their axis of rotation horizontal. Compare, for example, the unstable vortex pattern of frame (1,1) in Fig. 14 with the stable pattern of frame (7,9). This may depend on the speed of rotation (the vortex strength) and/or the radius of the cylinders (distance between vortex centers). This analogy is one that has been applied to the wake behind a cylinder (i. e., a Karman vortex street). In addition, the animation of Fig. 15 clearly shows that the asymmetry begins in an annulus surrounding the vortex core where the type of interaction just discussed would occur.

Today's maneuvering demands on both aircraft and missiles has made the phenomenon of asymmetric separation more important then ever before. In the past research was simply directed toward delaying the phenomenon to higher angles of attack. Today's research is intended to harness the yawing force produced by the phenomenon to supplement lost rudder effectiveness at high α. A yawing moment is produced by the side force generated by asymmetrically disposed vortices near the vehicle nose. If a device could be placed at the nose tip to control the direction of this side force rudder power would be supplemented at high α. Grumman's X-29 has

already demonstrated this capability in flight tests (Ref 32). An important extension of the current research is in the area of using vortex asymmetry as a control device at high angle of attack. A more fundamental understanding of the phenomenon is necessary to be able to use it effectively and reliably. In the flight tests of Ref. 32, small thrusters were used successfully to control asymmetric flow. If a more subtle device were to be used, a deeper understanding of the phenomenon would be required. A subtle device would have quick response time and be cheap and easy to install on existing vehicles. Devices such as very small vanes, flaps, or even piezo-electric devices could be used to control vortex asymmetry. The yaw control gained from minute deflection would make these very powerful devices. In order to use these very subtle schemes, a more detailed understanding of all the parameters affecting the phenomenon must be available.

The work of Thomas (Ref 19) showed a significant effect of conical Reynolds number (Reynolds number based on the distance from the apex of the cone) on the asymmetry of the flow about a 5-deg circular cone at $M_\infty = 1.8$ and $\alpha = 20°$. It was reported (Ref 19) that as the local Reynolds number is reduced below 10^6, the side force is reduced, and at a critical Reynolds number of 30,000, the side force is zero. Figure 16 shows the variation in critical Reynolds number with free-stream Mach number for a 5-deg circular cone at $\alpha = 18°$. Associated with a critical Reynolds number (R_{ecr}) is a critical length scale $R_{ecr}v_\infty/U_\infty$. It was reported in Ref 19 that if an asymmetry in the nose geometry of a three-dimensional body exists and if the Reynolds number based on a length scale associated with this disturbance is supercritical (in the conical sense), the fully three-dimensional flow will be asymmetric. In the inviscid limit $v_\infty \rightarrow 0$, the critical length scale vanishes and any infinitesimal asymetric disturbance at the nose will result in asymmetric flow. This result is consistent with the findings of Ref 7 and 14. It is interesting to compute the critical length scales for air at 10,000-ft altitude at the two limits of Fig. 16, $M_\infty = 1.2$ and $M_\infty = 3$. At $M_\infty = 1.2$ it is 0.02 in. and at $M_\infty = 3$ it is 0.07 in. These numbers are very small in comparison to a 60-ft fighter aircraft or even a 5-ft long missile. This implies that asymmetries in the first 0.002%→0.1% of an aircraft or missile nose will cause an asymmetric vortex pattern, which in turn will result in a large side force. Presumably asymmetric perturbations of this same order of magnitude can control the direction of the side force. Conceivably the design goal of any control device will be to overcome the "natural" asymmetry built into the nose (i. e., the asymmetry due to manufacturing tolerances). Finally, the placement of the control may be critical. It

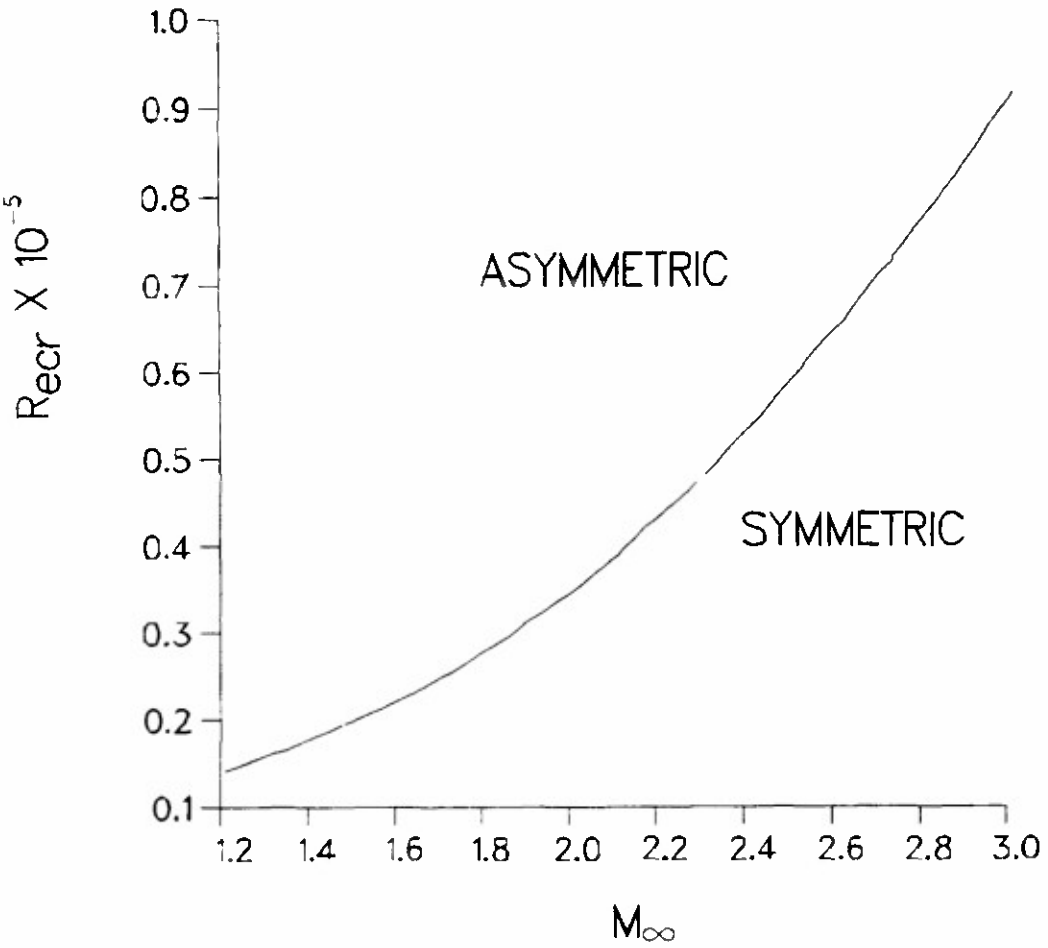

Fig. 16 Critical Reynolds Number as Function of Mach Number ($\delta = 5°$, $\alpha = 18°$)

would seem that the device must affect the flow in the first 0.002%→0.1% of the vehicle in order to be effective. The next phase of the current research project is intended to answer these questions by gaining a deeper understanding of all the parameters affecting the phenomenon.

The research reported on here has investigated the origin of the instability in the symmetric conical flow about pointed bodies at high angle of attack. This research was founded on the assumption of conical flow for good reason. The conical flow assumption reduces the problem to a two-dimensional one, thereby making it trackable from a computational point of view. In addition, the close relationship between the conical computational results and experimental data (see, for example, Fig. 2) proves that some aspects of the physics are captured in the conical governing equations. There is no question but that the conical equations can be used effectively in many scientific/engineering investigations into this phenomenon. In particular, the discussion of the previous paragraph shows how conical computations can be used to set design requirements for any system intended to control vortex asymmetries effectively. In the next phase of the current research project the conical equations would be used to determine the critical length scale ($R_{ecr}v_\infty/U_\infty$) as a function of geometry (cone angle and cross-sectional shape) and angle of attack. These studies would be preceded by a careful evaluation of accuracy of these conical computations. In Ref 19 it was noted that the critical Reynolds number was somewhat sensitive to grid resolution. All the work in this area (experimental, analytical, and computational) has indicated that the flow under consideration is sensitive to small changes in many of the parameters of the problem. The first step in a computational effort is to be sure that all the parameters affecting the phenomenon are of a physical nature and not significantly affected by numerical error.

The conical assumption can not be used to understand all aspects of this phenomenon. Some fully three-dimensional computations must be used. The problem with all the fully three-dimensional Navier-Stokes computations carried out thus far has been uncertainties near the treatment of nose tip (Ref 16-20). These uncertainties may not cause major inaccuracies in "standard" flow situations but by now it should be obvious that the nose tip region is critical to the accuracy of the computation of asymmetric separated flow. The fully three-dimensional computations proposed as part of the next phase of the current research effort will concentrate on the accurate

computation of the nose region. The only model for this region which can resolve the details of the flow is one in which the nose is assumed blunt. This is the only way to resolve the development of the boundary layer in this region. It has been shown experimentally (Ref 2) that nose blunting has a significant effect on the phenomenon of asymmetric separation. Only by assuming the nose blunt and resolving this bluntness can this effect be controlled. Figure 17 shows the grid that would be used to resolve this phenomenon properly. Figure 17a shows the global grid while Fig. 17b shows the grid in the vicinity of the nose tip. With this grid the development of the boundary layer will be resolved properly. For the first time, the impact of the details of the development of the boundary layer on asymmetric separation will assessed. The computational results of Ref 16 to 20 in essence let the numerics blunten the nose tip with artificial dissipation. Secondly, in light of the results of Ref 15, it is obvious that any numerical result not converged to machine zero is suspect. All iterations in the three-dimensional computations of the proposed effort will be continued to machine zero. Finally, numerical inaccuracies in the three-dimensional calculations will be monitored with grid refinement studies.

The proposed continuation of this research is intended to determine the magnitude and the nature of perturbations required to control asymmetric separation, thereby making a direct impact on the design of devices capable of controlling this phenomenon. The flows considered during the next phase of this project will again be steady. The study of unsteady flow effects and their impact on the development of any control system (i. e., feedback loops) will be the subject of future proposals.

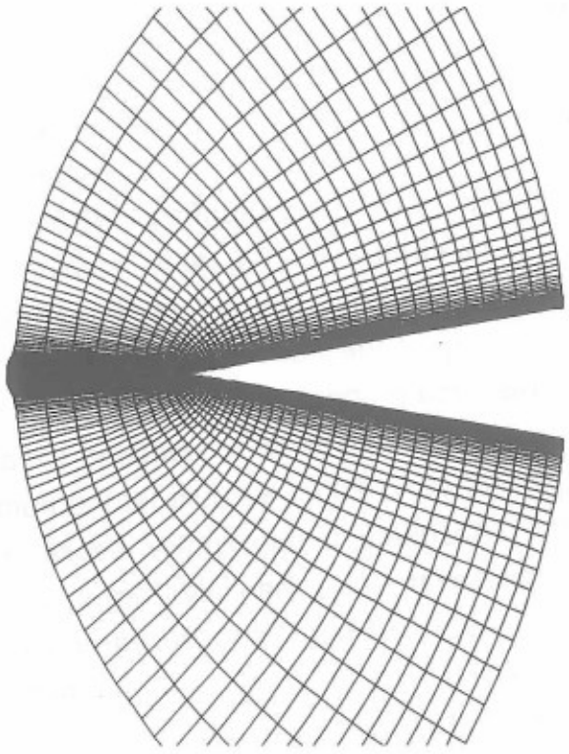

(a) Globel Grid

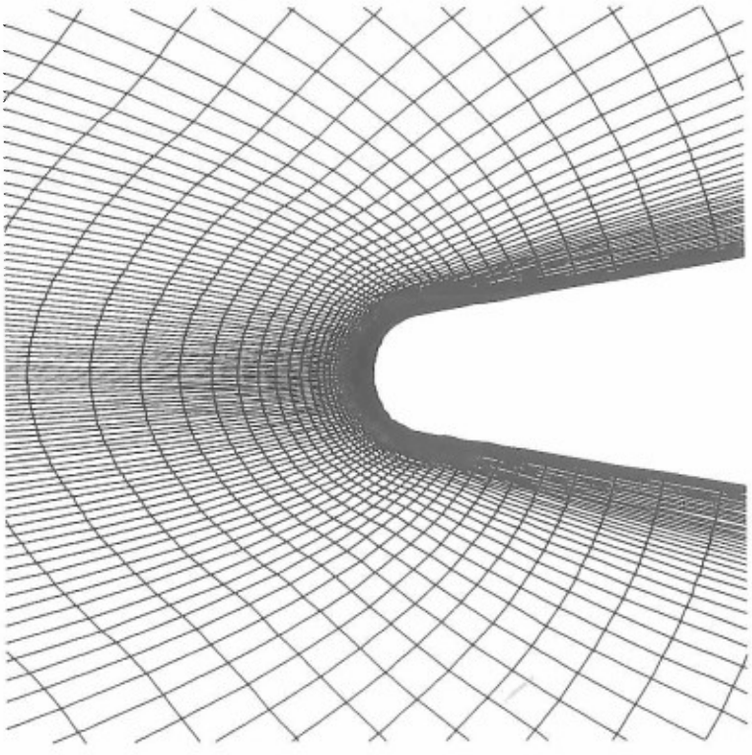

(b) Grid at Tip

Fig. 17 Grid Designed to Resolve Tip of Blunt 10° Cone

4. REFERENCES

1. Rao, P.M., "Side-Force Alleviation on Slender, Pointed Forebodies at High Angles of Attack," AIAA Paper 78-1339, 1978.

2. Moskovitz, C.A., Hall, R.M., and Dejarnetti, F.R., "Effects of Nose Bluntness, Roughness and Surface Perturbation on the Asymmetric Flow Past Slender Bodies at High Angle of Attack," AIAA-89-2236, 1989.

3. Fellows, K.A., and Carter, F.D., "Results and Analysis of Pressure Measurements on Two Isolated Slender Wings and Slender Wing-Body Combinations at Supersonic Speeds, Vol. 1 -- Analysis," ARA Rept. 12, 1969.

4. Peake, D.J. and Owen, F.K., "Control of Forebody Three-Dimensional Flow Separation," AGARD-CP-262, pp 15-1 to 15-26, 1979.

5. Hall, R.M., "Influence of Reynolds Number on Forebody Side Forces for 3.5 - Diameter Tangent-Ogilve Bodies," AIAA Paper 87-2274, 1987.

6. Kenner, E.R., Chapman, G.T., and Kruse, R.L., "Effects of Mach Number and Afterbody Length on the Onset of Asymmetric Forces on Bodies at Zero Sideslip and High Angles of Attack," AIAA Paper 76-66, 1976.

7. Dyer, D.E., Fiddes, S.P., and Smith, J.H.B., "Asymmetric Vortex Formation from Cones at Incidence - A Simple Inviscid Model," Aeronautical Quarterly, Vol. 33, pp 293-312, 1982.

8. Bryson, A.E., "Symmetrical Vortex Formation on Circular Cylinders and Cones," J. Appl Mech (ASME), Vol 26, pp 643-648, 1959.

9. Fiddes, S.P., "Separated Flow About Cones at Incidence -- Theory and Experiment," Proc of Symp on Studies of Vortex Dominated Flow, NASA/LRC, 1985.

10. Smith, J.H.B., "Behavior of a Vortex Sheet Separating from a Smooth Surface," R.A.E. TR77058, 1977.

11. Marconi, F., "The Spiral Singularity in the Supersonic Inviscid Flow Over a Cone," AIAA Paper 83-1665, 1983.

12. Marconi, F., "Flat Plate Delta Wing Separating Flows with Zero Total Pressure Losses," AIAA Paper 87-0038, 1987.

13. Marconi, F., "Fully Three-Dimensional Separated Flows Computed with the Euler Equations," AIAA Paper 87-0451, 1987.

14. Marconi, F., "Asymmetric Separated Flows About Sharp Cones in a Supersonic Stream," Proc of the 11th International Conf on Numerical Methods in Fluid Dynamics, Williamsburg, VA, 1988.

15. Siclari, M.J. and Marconi, F., "The Computation of Navier-Stokes Solutions Exhibiting Asymmetric Vortices," AIAA Paper No. 89-1817, presented at the AIAA 20th Fluid Dynamics, Plasma Dynamics and Lasers Conf, Buffalo, NY, June 1989.

16. Degani, D. and Schiff, L.B., "Numerical Simulation of the Effect of Spatial Disturbances on Vortex Asymmetry," AIAA Paper No. 89-0340, presented at AIAA 27th Aerospace Sciences Mtg, Reno, NV, Jan 1989.

17. Kandil, O.A., Wong, T.C., and Liu, C.N.,"Prediction of Steady and Unsteady Asymmetric Flows Around Cones," AIAA 90-0598, presented at AIAA 28th Aerospace Sciences Mtg, Reno, NV, Jan 1990.

18. Rosen, B.S. and Davis, W.H., "Numerical Study of Asymmetric Air Injection to Control High Angle-of-Attack Forebody Vortices on the X-29 Aircraft," AIAA 90-3004-CP, Aug 1990.

19. Thomas, J.L.,"Reynolds Number Effects on Supersonic Asymmetric Flows over a Cone at High Angle of Attack," AIAA 91-3295, presented at AIAA 9th Applied Aerodynamics Conf, Baltimore, MD, Sept. 1991.

20. Hartwich, P.M. Hall, R.M., and Hersch, M.J., "Navier-Stokes Computations of Vortex Asymmetries Controlled by Small Surface Imperfections," AIAA Paper 90-0385, 1990.

21. Zillac, G.C., Dagani, D. and Tobak, J., "Asymmetric Vortices on a Slender Body of Revolution," AIAA Paper 90-0388, 1990.

22. Williams, D. and Bernhardt, J., "Proportional Control of Asymmetric Vortices with the Unsteady Bleed Technique," AIAA Paper 90-1629, 1990.

23. Siclari, M.J., DelGuidice, P., and Jameson, A., "A Multigrid Finite Volume Method for Solving the Euler and Navier-Stokes Equations for High Speed Flows," AIAA Paper No. 89-0283, presented at the AIAA 27th Aerospace Sciences Mtg, Reno, NV, Jan 1989.

24. Siclari, M.J., and DelGuidice, P., "A Hybrid Finite Volume Approach to Euler Solutions for Supersonic Flows," AIAA Paper No. 88-0225, presented at the AIAA 26th Aerospace Sciences Mtg, Reno, NV, Jan 1988.

25. Jameson, A., "A Vertex Based Multigrid Algorithm for Three-dimensional Compressible Flow Calculations," presented at the ASME Symp on Numerical Methods for Compressible Flow, Anaheim, CA, Dec 1986.

26. Thomas, J.L., Van Leer, B., and Walters, R.W., "Implicit Flux-Split Schemes for the Euler Equations," AIAA Paper No. 85-1680, presented at the AIAA 18th Fluid Dynamics and Plasmadynamics and Lasers Conf, Cincinnati, Ohio, July 1985.

27. Schlichting, H., *Boundary Layer Theory*, McGraw Hill, 1951, pp 382-400.

28. Hannemann, K. and Oertel, H., "Numerical Simulation of the Absolutely and Convectively Unstable Wake," Journal of Fluid Mechanics, 199, 1989, pp 55-88.

29. Oertel, H., "Wake Behind Blunt Bodies," Annual Review of Fluid Mechanics, Vol 22, 1990.

30. International Mathamatics and Statistics Library, *MATH/LIBRARY FORTRAN Subroutines for Mathematical Applications*, Version 1.1 (IMSL, Houston, Jan 1989), pp 289-300.

31. Siclari, M.J., Federico, P.and Mandel, M., "Visualization Research at Grumman's Computer Application Laboratory (CAL)," presented at the SAE Aerospace Technology Conf and Exposition, Long Beach, CA, Oct 1990.

32. Krumenacker,J. and Pellicano, P., "Flight Simulation and Data Analysis During A High Angle of Attack Vortex Flow Control Flight Test Program," AIAA Paper No. 92-4108, presented at the AIAA 6th Flight Test Conf, Hilton Head Islang, SC, August 1992.

33. Raghu, S., "The Effect of a Small Rotating Forebody on the Development of Longitudinal Vortices on a Slender Cone," presented at the APS 44th Annual Mtg of the Division of Fluid Dynamics, Nov 1991.

34. Fidler, J.E., "Active Control of Asymmetric Vortex Effects", AIAA Journal of Aircraft, Vol 18, No. 4, 1981.

35. Raghu, S., private communications, 1992.

APPENDIX A -- INVESTIGATION OF TIP SPINNING

An experimental investigation at SUNY at Stony Brook (Ref 33) uncovered a signiticant effect of nose spinning on asymmetric separation. There have been in the pasf studies of vortex control by nose spinning [34] but none as dramatic as that of Ref 33. The vortices in the lee plane of a cone cylinder af high angle of attack are illuminated by a laser sheet places 0.5 meter from the apex. The first centimeter of the model is made to spin with a variable speed motor inside the model. The angle of attack is supercritical (i. e., the separated flow is asymmetric) at zero spin rate. The laser sheet shows clearly that the flow is asymmetric as the nose begins to spin. At low spin rates the flow, which had been steady at zero spin rate, becomes unsteady. Suddenly, at a particular spin rate, the flow becomes steady again and the vortices are symmetric.

This experiment could only be approximated with the current conical Navier-Stokes computation. The surface boundary was modified to allow for a specified tangential speed. This is not a model of a spinning nose since the surface speed in a solid cone rotation would vary with axial location. Nonetheless, the results of this approximate computation are very interesting. As the surface speed was increased, the asymmetry was indeed reduced. Figure A-1 compares the entropy contours (which clearly show the vortices) for a zero fangential speed and 0.25X the free stream of sound. The reduction in the asymmetry is obvious. Figure A-2 shows the variation in side force as a function of surface speed. At zero spin rate three solutions exist: C_Y = -0.25, C_Y = 0.25 (fhe two mirror image solutions), and the symmetric unstable C_Y = 0 solution. As the spin rate is increased from zero, starting from the C_Y = -0.25 flow, the side force is decreased. Once fhe minimum value of -0.1 (at a spin rate of 0.25) is reached, it can no longer be reduced. If fhe spin rate is increased ever so slightly, the side force jumps to a value of almost 0.3. The very asymmetric flow for this condition is shown in Fig. A-3. If fhe spin rate is decreased starting from this condition, the side does not return to its negafive values but remains posifive. The hysteresis loop associated with this phenomenon is shown clearly in Fig. A-2. It must be pointed out that solutions connecting the two branches of the hysteresis loop (the dashed line of Fig. A-2) are all unstable and could not be computed (except for C_Y = 0 by imposing symmetry). A phenomenon similar to that described here has recently been noted experimentally [35]. The effect of nose spinning on high angle-of-attack

asymmetric flow and this apparent hysteresis loop should be the subject of future research.

(a) $V_T/a_\infty = 0$ (b) $V_T/a_\infty = 0.25$

Fig. A-1 Entropy Contours Tangential Speed = 0 & 0.25X Free-Stream Speed of Sound ($M_\infty = 1.8$, $\delta = 5°$, $\alpha = 20°$, $R_\theta = 10^5$)

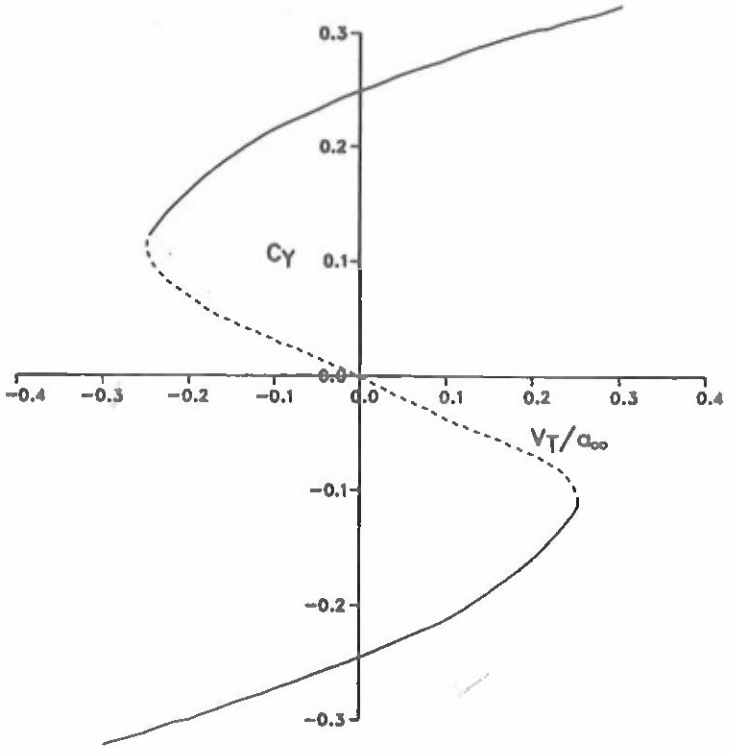

Fig. A-2 Variation of Side Force with Tangential Speed ($M_\infty = 1.8$, $\delta = 5°$, $\alpha = 20°$, $R_\theta = 10^5$)

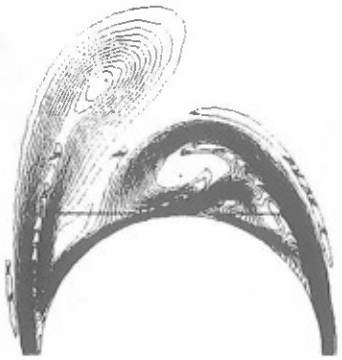

Fig. A-3 Entropy Contours Tengential Speed 0.25X Free-Stream Speed of Sound, Positive Side Force ($M_\infty = 1.8$, $\delta = 5^\circ$, $\alpha = 20^\circ$, $R_\theta = 10^5$)